



The Anthropogenic Influence on Glacier Retreat in Central Chile

Karina Vallejos¹, Lina Castro¹, Alvaro Ossandon¹, Raúl Flores¹, and Felipe McCracken¹ Departamento de Obras Civiles, Universidad Técnica Federico Santa María, Valparaíso, Chile.

Correspondence: Lina Castro (lina.castro@usm.cl)

Abstract. Glaciers in the Andes mountain range have retreated since the mid-20th century. This change has been attributed to climate change and the effects of local pollution. Some glaciers subjected to similar meteorological conditions and the same influence of climate change are found to exhibit significantly different retreat rates, which cannot be explained by climatological factors alone. In the Maipo River basin, located in central continental Chile, two glaciers with similar climatic and geomorphological characteristics, the Paloma Oeste Glacier (POG) and the Bello Glacier (BG), exhibit significantly different levels of ablation. We implement two multivariable regression models, one per glacier, to identify the importance of specific climatic and anthropogenic variables in glacier surface area retreat. These models incorporate a temperature-related variable and precipitation (indicative of climate change), surface-level Black Carbon concentration (BC, indicative of anthropogenic activity) and the large-scale climate indices PDO and Niño 3.4 (related to climate variability) as covariates. The results indicate that the glacier surface change is more sensitive to the surface BC concentration and the Niño 3.4 index than to precipitation, PDO, or temperature for both glaciers. However, since the surface BC concentration in POG is more than 40 times higher than in BG, the area retreat is significantly higher in POG than in BG. Between 2000 and 2020, 49% of the area retreat of POG is explained by BC pollution, while 97% of BG's retreat is explained by climatic effects (climate change and climate variability). Furthermore, when analyzing the causes of glacier retreat in POG before and during sustained drought conditions, often referred to as the Central Chile Megadrought (2010-2020), we found a change in the relative importance of BC surface concentrations. Before the Megadrought, BC is identified as the leading cause of glacier retreat in POG, accounting for a 53%. However, the climatic effects (61%) on glacier retreat during the Megadrought become more relevant than the impact of BC (39%). These results highlight the spatiotemporal varying influence of climatic and anthropogenic factors on glacier retreat, emphasizing the significant contribution of climate change, particularly during sustained drought conditions.

20 1 Introduction

The Andes mountain range represents the largest freshwater reservoir in Chile, where significant amounts of water are stored as glacier ice and snow (Barcaza et al., 2017; Dangles et al., 2017; Farías-Barahona et al., 2020; Masiokas et al., 2020). Caro et al. (2020) identified a glacierized area of approximately 2168 km² in Chile, 4.54% of which is located in the Central Andes region (32–36°S). These glaciers play a crucial role in water availability throughout Central Chile, contributing significantly to runoff during summer and fall, especially in dry years (Ayala et al., 2016; Escanilla-Minchel et al., 2020; Mernild et al., 2015; Ohlanders et al., 2013; Rodriguez et al., 2016). For example, on an annual scale in the Maipo basin, one of the largest





Andean basins in Central Chile containing Chile's largest city and capityal Santiago, glacier melt runoff accounts for 16% of total discharge, reaching up to 59% during the summer (Ayala et al., 2020). However, these glacier runoff rates have been affected by climate change and, in recent years, by sustained drought conditions (2010-present) often referred to as the Central Chile Megadrought (Masiokas et al., 2020; Dussaillant et al., 2019; Garreaud et al., 2020). In recent decades, glacier runoff has decreased in magnitude due to a combination of reduced precipitation in the Andes (Boisier et al., 2016) and a decline in glacier ice volume (Ayala et al., 2016, 2020; Casassa et al., 2009; Mernild et al., 2015). During the ongoing drought, glacier runoff in the Maipo Basin has accounted for 17% of annual discharge and 55% of summer discharge (Ayala et al., 2020).

Since the mid-20th century, most glaciers in the central Andes have undergone geometric changes, with reductions in both area and thickness, that is, they have experienced glacier retreat (Le Quesne et al., 2009; Farías-Barahona et al., 2019; Masiokas et al., 2020; Farías-Barahona et al., 2020). A notable example is the Echaurren Norte Glacier in Central Chile, which has lost approximately 20 meters of water equivalent (mwe) since 1975/76, a critical loss that places it at risk of disappearing within the next few decades (Farías-Barahona et al., 2019). El Morado Glacier, located in the Central Andes, had lost 40% of its glacierized area by 2019 (Farías-Barahona et al., 2020). In fact, Masiokas et al. (2020) showed that glaciers in the Central Andes exhibit a more accelerated melt rate than those in other parts of the Andes, due to a susteained decreasing trend in precipitation that has clearly intensified since 2010 with the onset of the Megadrought (Garreaud et al., 2017; Rabatel et al., 2011). For example, in the desert region of the Andes (17.5°-31°S), annual glacier retreat rates remained relatively stable before and after 2009 (0.00 \pm 0.22 mwe \cdot year⁻¹ for 2000–2008, and -0.11 \pm 0.20 mwe \cdot year⁻¹ for 2009–2017). In contrast, glaciers in the Central Andes showed stable to positive change rates of $0.17 \pm 0.23 \text{ mwe} \cdot \text{year}^{-1}$ between 2001 and 2008, but negative and significant rates of $-0.40 \pm 0.21 \; \mathrm{mwe \cdot year^{-1}}$ between 2009 and 2017 (Dussaillant et al., 2019). Malmros et al. (2016) analyzed the retreat of the Olivares Alfa Glacier (GOA) and Juncal Norte (JN) located in the same Central Andes region, and found that GOA lost 63% of its glacier ice area between 1955 and 2013, while JN lost only 10%. Lo Vecchio et al. (2022) evaluated the glacier area of the Maipo volcano based on four decades of satellite records (1976–2020), during which the glacier area decreased by 63% from its original extent. Glaciers have provided a significant portion of freshwater to rivers in central Chile; however, due to changing climate conditions and the ongoing Megadrought, this percentage has increased at the cost of an unsustainable imbalance caused by the ablation of 59% of the glacier area in the region. This ablation has not been offset by new snowfall (McCarthy et al., 2022).

Several studies propose that changes experienced by the cryosphere in recent years are due to climate change (Rivera et al., 2006; Raina, 2009; Migliavacca et al., 2015; Valdés-Pineda et al., 2014). However, evidence shows that glacier retreat differs among glaciers in areas with similar climatic conditions (e.g., Cereceda-Balic et al., 2022). This fact highlights that it is not only current and future climate conditions that are threatening the Andean cryosphere. Shaw et al. (2021) reported a significant negative trend in glacier albedo in central Chile. This trend was particularly pronounced during the 2010–2020 period and has impacted glacier melt, especially under severe drought conditions. Emissions of black carbon (BC) and suspended particulate matter (PM) reduce snow and ice albedo, increasing radiative forcing on the surface and thereby leading to accelerated melting (Cereceda-Balic et al., 2018; Li et al., 2020; Ming et al., 2009; Kang et al., 2020; Qu et al., 2014; Zhang et al., 2020). Cereceda-Balic et al. (2018) also documented a reduction in snow albedo due to BC and PM emissions from vehicles near the high-



70



mountain cryosphere in the Portillo sector (Central Chile), with a reduction of 0.08 albedo units per day under heavy traffic conditions (approximately 2000 vehicles per day). In an effort to understand the origin of differences in glacier retreat in central Chile and their relationship with BC and PM, Cereceda-Balic et al. (2022) compared two morphologically similar glaciers, Olivares Alfa Glacier (OAG) and Bello Glacier (BG), in the Maipo basin. They related the surface concentration of Black Carbon (BC) to the rate of area retreat. Their results showed that OAG, which exhibited greater glacier retreat, had a higher surface concentration of BC compared to BG. The impact on glacier area retreat in OAG is mainly attributed to mining activities, which account for 82% of the total retreat. The remaining 18% corresponds to the effect of climate change, highlighting the significant role of local pollution in glacier melt in this part of the Andes and its implications for water resources.

Glaciers in central Chile show a significant retreat, which must be evaluated with particular attention to the causes, both climatic and anthropogenic. Glaciers are that are close to each other and therefore subjected to similar climatic conditions differ in their retreat rates, a dynamic that does not appear to be explained by glaciological factors alone (Cereceda-Balic et al., 2020; Le Quesne et al., 2009; Malmros et al., 2016). The main objective of this study is to identify the factors that drive the accelerated glacier retreat observed in Central Chile by quantifying the percentage contribution of each factor to the reduction in glacier area between the hydrological years 2000 and 2020. To this end, a multiple linear regression model is proposed to identify the relationship between predictors (climatic and anthropogenic variables) and the annual variations in glacier area. We select two glaciers that share climatic and geomorphological similarities and define the climatic and anthropogenic variables that are correlated with the observed retreat. The glaciers selected for analysis were POG and BG, both located in central Chile but with different ablation rates between 2000 and 2020: -1.2% and -0.6%, respectively. POG has retreated at a rate of -1.08% between 1955 and 2013 (Malmros et al., 2016), while BG has retreated at a rate of 0.51% between 2004 and 2014 (Cereceda-Balic et al., 2022). The climatic variables used as predictors included the number of days with average temperatures below 0°C, accumulated precipitation over the hydrological year, and the macroclimatic indices PDO and Niño 3.4. The anthropogenic variable considered was surface-deposited Black Carbon (BC), as BC is one of the primary products of anthropogenic activities (e.g., combustion). The paper is organized as follows: Section 2 describes the study area, data collection and analysis methods. Section 3 presents the results and discusses the findings. Finally, conclusions are presented in Section 5.

2 Study Area and Methods

2.1 Study Area

We selected the Paloma Oeste and Bello glaciers, located in the headwaters of the Maipo River basin. These glaciers account for 4.54% of the glacierized area in central Chile. Together, these glaciers contribute approximately 59% of the total runoff during the summer and early fall months (2010–2016; Ayala et al., 2020). The Maipo River basin features a temperate Mediterranean climate, characterized by a prolonged dry season and cold high-altitude conditions in the Andes Mountains, with peak temperatures during summer and most precipitation occurring in winter (DGA, 2004). Between 1961 and 2022, the temperature in the upper basin has increased at a rate of +0.3°C per decade, doubling the national average warming rate of +0.15°C



105

110

115



(DGA, 2022). Annual precipitation in the Maipo basin has decreased by approximately 15% per decade over the same period (DGA, 2022). Hydrologically, the basin exhibits a mixed regime, with direct precipitation in the lower zone and contributions from snow and glacier melt in the upper zone.

The Maipo River basin contains 979 individual glaciers, ranging in surface area from 0.1 km² to 23 km², and covering a total area of 387.4 km². This accounts for 2.55% of the total basin area and 6.6% of the mountainous zone. Glaciers are generally distributed at elevations between 2,640 and 5,650 meters above sea level (DGA, 2014). The basin contains both debris-covered and clean-ice glaciers, encompassing a variety of glacier types such as rock glaciers, valley glaciers, mountain glaciers, and glacierets. Regarding glacier orientation, most glaciers have south-facing aspects; according to the inventory by Marangunic (1979), only 4% of the glaciers are oriented toward the north.

Figure 1 shows the POG and BG glaciers analyzed in this study. These glaciers were selected based on an evaluation of existing glaciers considering geomorphological characteristics—such as mean elevation, accumulation zone orientation, ablation zone orientation, and overall glacier aspect—as well as glacier retreat patterns, mass balance data, and atmospheric pollution records (DGA, 2011, 2014; Ayala et al., 2016; Malmros et al., 2016; Barcaza et al., 2017; Segovia Rocha and Videla Giering, 2017; Farías-Barahona et al., 2019; Cereceda-Balic et al., 2022; Farías-Barahona et al., 2020). The two selected glaciers are located within the same climatic zone and exhibit similar morphological characteristics, yet they have experienced markedly different retreat rates in recent years. Table 1 shows that glacier characteristics such as elevation, mean, minimum, and maximum altitude and orientation are quite similar for both glaciers. In terms of slope, POG exhibits a steeper gradient than BG. However, studies in glacier geomorphology associate glacier slope with flow velocity and, consequently, with glacier dynamics, while properties such as altitude and orientation are considered more influential in determining glacier mass balance behavior (Evans, 2013).

Table 1. Geomorphological characteristics of BG and POG. Hmin, Hmax, and Have correspond to the minimum, maximum, and mean elevations (in meters above sea level), respectively. Accumulation and Ablation Orientation indicate the predominant orientation of the accumulation and ablation zones.

Name	Glacier Type	Basin	Sub-basin	Hmin (masl)	Have (masl)	Hmax (masl)	Accumulation Orientation	Ablation Orientation	Overall Orientation	Slope (°)
BG	Mountain glacier	Rio Maipo	Rio Yeso	3987	4439	4917	SSE	SSE	S	17.6
POG	Mountain glacier	Rio Maipo	Rio San Francisco	3704	4405	4887	S	SW	S	30.0

Figure 1 shows that POG is located near two copper mining operations, whereas BG far from anthropogenic activities. (Gramsch et al., 2020) conducted a study on Black Carbon transport between Santiago, Chile, and high-mountain glaciers between 2014 and 2015, revealing higher concentrations of Black Carbon in La Parva—a high-altitude area—compared to





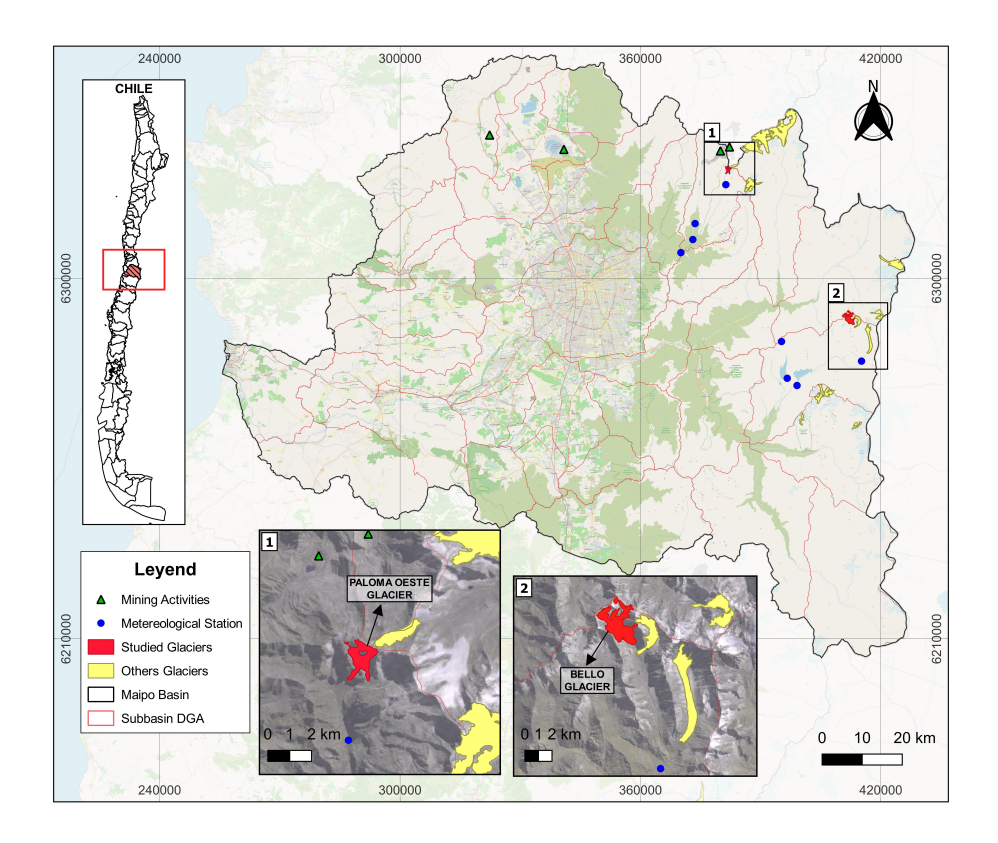


Figure 1. Maipo River basin, location of selected glaciers (POG and BG), nearby anthropogenic activity, and meteorological stations.

other nearby glaciers. La Parva is located at 2800 meters above sea level, near glaciers in the northern sector of the Maipo basin. The study by Gramsch et al. (2020) found that 25–37% (summer–winter) of the pollution in La Parva area was due to nearby mining activity, while approximately 50% was attributed to BC transported from Santiago. This information was fundamental in selecting the glaciers for this study, as POG is located near La Parva, the area with the highest recorded levels of atmospheric pollution. In contrast, BG is located in the region of the Maipo basin characterized by the lowest level of high-mountain pollution.

2.2 Database

120

The selection of climatic and anthropogenic variables as potential drivers of glacier ablation was guided by previous studies conducted in the region (Gramsch et al., 2020; Cereceda-Balic et al., 2020; Cordero et al., 2022). The selected variables include climate indicators (precipitation and temperature), measures of climate variability (macroclimatic indices such as EL Niño 3.4 and the Pacific Decadal Oscillation, PDO), and an atmospheric pollution proxy (deposited Black Carbon, BC). The time series of these variables were analyzed for the hydrological years 2000 to 2020, considering that the hydrological year in Chile runs from April 1 to March 31 of the following year.





2.2.1 Landsat

Landsat TM, ETM+, and OLI/TIRS satellite images (from Landsat 5, 7, and 8, respectively) were downloaded for each summer season (December to March) in the study period, to estimate glacier area while excluding seasonal snow. The glacier surface was derived by calculating the Normalized Difference Snow Index (NDSI), as shown in Eq. (1), and manually validating the delineated area using QGIS software. NDSI values greater than 0.4 are generally considered indicative of snow presence (Dozier, 1989). Table 2 presents the details of the satellite images analyzed. For 2012, two Landsat 7 ETM+ images were used to correct the SLC-off issue (Striping Noise Correction Loss-off), following the method proposed by Chen et al. (2011). This issue originated in May 2003 due to thermal scanner malfunction of the sensor.

$$NDSI = \frac{(Green_{band} - Medium\ Infrared_{band})}{(Green_{band} + Medium\ Infrared_{band})} \tag{1}$$

2.2.2 Weather Records

140

160

To assess the effects of climate change, time series of precipitation and temperature were analyzed for each glacier over the observation period. The meteorological stations used for this analysis are listed in Table 3 and shown in Figure 1. Precipitation data were extrapolated from nearby meteorological stations for each glacier, allowing estimation of annual totals for each hydrological year. The meteorological stations used were "Yeso Embalse" for BG and "Estero Yerba Loca antes Junta San Francisco" for POG. Additional stations were employed to fill data gaps when necessary. For temperature, the analysis focused on the number of days per hydrological year with daily mean temperatures below 0°C at the average glacier elevation. This time series was constructed by extrapolating daily temperature data from each glacier's reference meteorological station to its mean elevation. The selection of the 0°C threshold temperature variable—hereafter referred to as DTbCero (Days with Temperature below Zero)—is supported by its prior use in global studies on glacier response to climate change, where 0°C is considered the melting point of ice (Vincent, 2002; Wiltshire, 2014).

2.2.3 Large-Scale Climate Indices

The macroclimatic indices considered in this study are two of the most influential factors affecting precipitation and temperature regimes in central Chile: Niño 3.4, which is one of the key indices associated with the El Niño—Southern Oscillation (ENSO) phenomenon (Trenberth, 1997; Núñez et al., 2013), and the Pacific Decadal Oscillation (PDO), a low-frequency modulator of ENSO-related variability (Andreoli and Kayano, 2005; Núñez et al., 2013). Different phases of the Niño 3.4 and the PDO are associated with variations in regional climate patterns, leading to increases or decreases in precipitation and corresponding temperature changes (Núñez et al., 2013). Specifically, the warm phase of ENSO tends to produce above-average precipitation and warmer temperatures in central Chile (Hernandez et al., 2022; Garreaud et al., 2009). Likewise, the warm (positive) phase of the PDO displays an ENSO-like spatial pattern and has been linked to increased precipitation and warmer conditions over subtropical latitudes (Garreaud et al., 2009; Núñez et al., 2013).



170



Table 2. Details of satellite images used in the analysis of glacier surface area variation between 2000 and 2020.

Year	Water year	Date	Satellite	Name
2001	2000	Mar-10	Landsat 5	LT05_L2SP_233083_20010310_20200906_02_T1
2002	2001	Feb-25	Landsat 5	LT05_L2SP_233083_20020225_20200905_02_T1
2003	2002	Mar-24	Landsat 7	LE07_L2SP_233083_20030324_20200915_02_T1
2004	2003	Mar-02	Landsat 5	LT05_L2SP_233083_20040302_20200903_02_T1
2005	2004	Mar-05	Landsat 5	LT05_L2SP_233083_20050305_20200902_02_T1
2006	2005	Feb-04	Landsat 5	LT05_L2SP_233083_20060204_20201008_02_T1
2007	2006	Mar-20	Landsat 5	LT05_L2SP_232083_20070320_20200830_02_T1
2008	2007	Feb-10	Landsat 5	LT05_L2SP_233083_20080210_20200829_02_T1
2009	2008	Feb-12	Landsat 5	LT05_L2SP_233083_20090212_20200828_02_T1
2010	2009	Jan-30	Landsat 5	LT05_L2SP_233083_20100130_20200825_02_T1
2011	2010	Feb-02	Landsat 5	LT05_L2SP_233083_20110202_20200823_02_T1
2012	2011	Jan-12	Landsat 7	LE07_L1TP_233083_20120112_20161203_01_T1
	2011	Feb-13	Landsat 7	LE07_L1TP_233083_20120213_20200909_02_T1
2013	2012	Apr-02	Landsat 8	LC08_L1TP_232083_20130402_20200913_02_T1
2014	2013	Jan-25	Landsat 8	LC08_L1TP_233083_20140125_20200912_02_T1
2015	2014	Jan-28	Landsat 8	LC08_L2SP_233083_20150128_20200910_02_T1
2016	2015	Jan-15	Landsat 8	LC08_L2SP_233083_20160115_20200907_02_T1
2017	2016	Mar-06	Landsat 8	LC08_L2SP_233083_20170306_20200905_02_T1
2018	2017	Feb-26	Landsat 8	LC08_L1TP_233083_20140125_20200912_02_T1
2019	2018	Feb-24	Landsat 8	LC08_L2SP_233083_20190224_20200829_02_T1
2020	2019	Feb-11	Landsat 8	LC08_L2SP_233083_20200211_20200823_02_T1
2021	2020	Jan-28	Landsat 8	LC08_L2SP_233083_20210128_20210305_02_T1

Previous studies have examined the lag times at which large-scale climate indices, such as the Niño 3.4 and the PDO, exhibit their strongest teleconnections with snow variability in central Chile (Escobar and Aceituno, 1998; Masiokas et al., 2006). Escobar and Aceituno (1998) linked solid precipitation in the Andean region of central Chile to Sea Surface Temperature (SST), showing that snow accumulation during winter tends to be above normal when the mean SST anomaly between May and August exceeds +1°C, while winters with SST anomalies below -0.5°C are generally associated with lower-than-normal snowfall. Additionally, Masiokas et al. (2006) correlated various macroclimatic indices with snowpack time series in the central Andes across different seasons, finding the strongest relationship for the Niño 3.4 index during the May–October period. Regarding the PDO, they found the highest correlation with snowpack between August and October, approximately one season before the glacier surface measurements derived from satellite imagery (Masiokas et al., 2006). Based on these findings, this study considers the average values from May to September (winter period) for the Niño 3.4 index and from





Table 3. Details of meteorological stations from the Chilean Water Directorate (DGA) used to construct time series of precipitation and DTbCero (Days with Temperature below Zero). Source: http://dga.mop.gob.cl.

Station	UTM N	UTM E	Temporal Resolution	Altitude (mbsl)	Available Data	Glacier Analyzed	Distance to Glacier
Yeso Embalse	6273246	399081	1963 - Present	2475	Temperature and precipitation	BG	21 km
Portezuelo Echaurren	6284245	395278	1979 - Present	3847	Temperature	BG	17 km
Termas Del Plomo	6280290	415966	2016 - Present	2981	Temperature and precipitation	BG	11 km
Laguna Negra	6274286	397293	1965 – Present	2780	Temperature and precipitation	BG	21 km
Glaciar Olivares Alfa	6328251	386440	2018 – Present	4230	Temperature	POG	5 km
Estero Yerba Loca antes Junta San Francisco	6309689	373072	1974 – Present	1350	Temperature and precipitation	POG	20 km
Estero Yerba Loca en Piedra Carvajal	6323390	381313	2013 – Present	3250	Temperature and precipitation	POG	4 km

August to October (spring period) for the PDO index. We obtained records for both indices from the National Oceanic and Atmospheric Administration (NOAA) (http://psl.noaa.gov).

2.2.4 The Copernicus Atmosphere Monitoring Service (CAMS)

BC (Black Carbon) is classified as sedimentable particulate matter (SPM). It remains in the atmosphere for a shorter time than other atmospheric pollutants and tends to deposit on surfaces (Wang et al., 2018). BC is the most critical anthropogenic absorbing aerosol, with a global mean radiative forcing of +0.04 (+0.02 to +0.09) Wm⁻² (Bond et al., 2013; Shi and Liu, 2019). When deposited on snow, BC can significantly reduce snow albedo, being 50 times more harmful than dust and up to 200 times more harmful than ash in lowering surface reflectivity (CETAM: Centro de Tecnologías Ambientales UTFSM, 2014).
CAMS (Copernicus Atmosphere Monitoring Service), implemented by the European Centre for Medium-Range Weather Forecasts (ECMWF), provides both retrospective and forecast data on atmospheric composition (https://atmosphere.copernicus.eu/) (Flemming et al., 2017; Granier et al., 2019). Among the retrospective datasets, BC deposition data are available either in teragrams (Tg) or as deposition flux in units of kg·m⁻²·s⁻¹. This dataset has a spatial resolution of 0.1° and a monthly temporal resolution. To represent each year in this study, we calculated annual averages of BC deposition per unit area, i.e., BC deposition divided by the area of each grid cell. CAMS data have not yet been validated in Chile due to the lack of continuous





ground-based BC measurements on snow surfaces. However, previous studies have compared CAMS BC data with ground-based measurements in other regions, reporting generally good correlations e.g., Prabhu et al., 2020.

2.3 Methodology

190

195

Figure 2 outlines the methodology used to evaluate the POG and BG glaciers and to identify the variables that most influence their retreat. First, an exploratory analysis of the independent variables is performed to identify climatic trends and potential correlations among variables. Second, for each glacier, a multiple linear regression model (MLRM) is fitted to the glacier area using a set of predictors, including indicators of climate change and variability, as well as contamination effects, selected during the exploratory analysis. This step is the most critical part of the study, as it enables the identification of the predictors that most influence variations in glacier area. Several statistical tests are applied to verify the regression assumptions and to validate the proposed MLRM. Although the MLRM is fitted using all selected variables, separate MLRMs are also implemented for each variable to evaluate their effect.

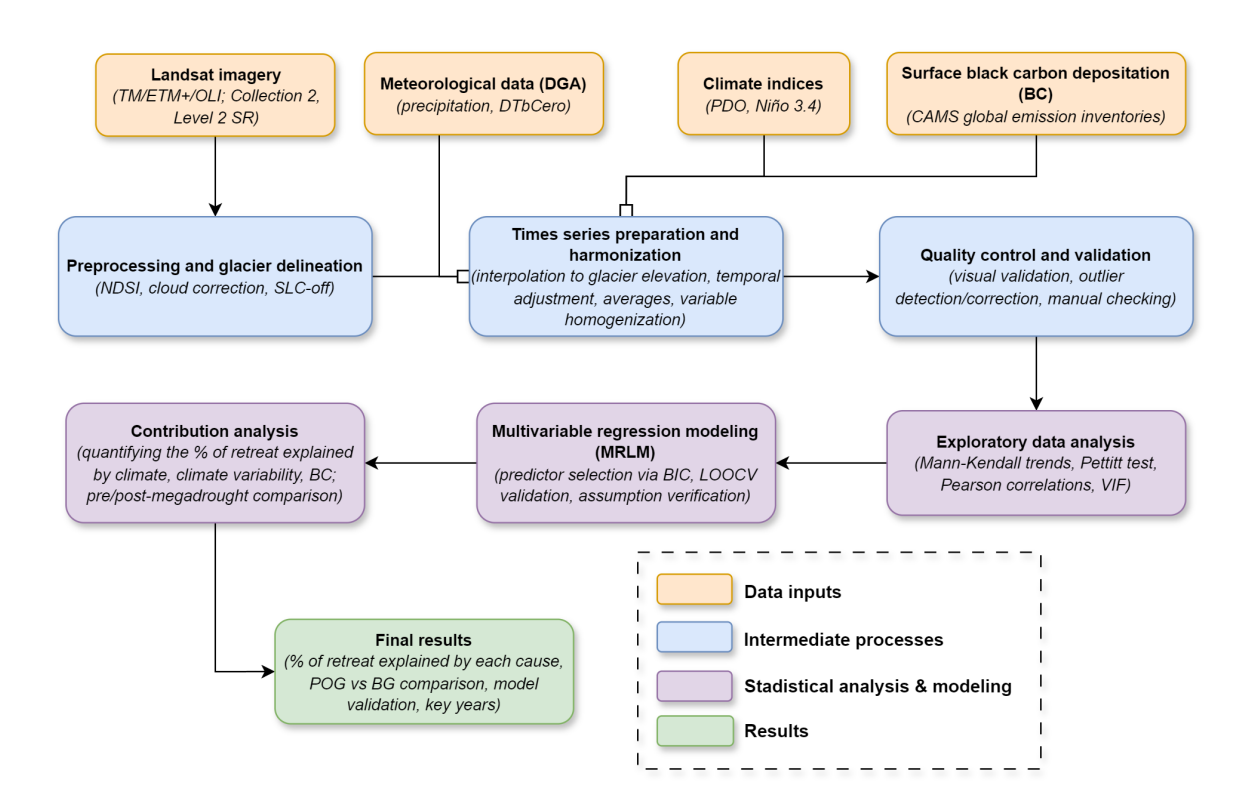


Figure 2. Workflow of the methodology used to analyze the retreat of the POG and BG glaciers and identify key climatic and anthropogenic drivers. The diagram summarizes data inputs, processing steps, statistical modeling, and contribution analysis.



200

205

215

220

225



2.3.1 Detection of Glacier Area

To refine glacier area estimates, we further filtered the Landsat images described in section 2.2.1 to exclude scenes with more than 20% cloud cover. After applying this filter, all remaining images were visually inspected to ensure they were cloud-free over the glacier areas of interest. For each year, we selected the image showing the largest glacier extent for subsequent analysis.

2.3.2 Exploratory Data Analysis

The exploratory data analysis aims first to identify temporal trends and time points at which these trends change across all studied variables. For this purpose, the Mann-Kendall test (MK; Kendall, 1957; Mann, 1945) and the Pettitt test (PT; Pettitt, 1979) were used, respectively. Subsequently, we calculated correlations between the predictor variables and the dependent variable (glacier area), as well as among the predictors themselves. These analyses help explore potential relationships between climatic patterns and pollution dynamics at the locations of both glaciers, and also serve to avoid multicollinearity among predictors in the MRLM. All statistical tests were conducted at a significance level of 5%.

2.3.3 Multiple Linear Regression Model

For each glacier (POG and BG), we fitted a multiple linear regression model (MLRM) to explain variations in glacier area using a set of predictor variables previously selected during the exploratory analysis. Models were built using both standardized and non-standardized data.

In the standardized models, the coefficients represent changes in the dependent variable (glacier area) expressed in standard deviations of each predictor. This approach enables a direct comparison of the relative sensitivity of glacier retreat to various variables. In contrast, non-standardized models allow for the quantification of impacts in the original measurement units. All fitted models follow the general form:

$$y = \beta_0 + \beta_1 X_1 + \beta_2 X_2 + \ldots + \beta_k X_k + \varepsilon \tag{2}$$

where y is the response or dependent variable; X_1, X_2, \ldots, X_k are the predictors; $\beta_0, \beta_1, \ldots, \beta_k$ are the regression coefficients; and ε is the residual or error term representing the difference between observed and predicted values. To standardize a model, both the dependent and independent variables are standardized. This yields standardized coefficients (β), which represent how much the response variable (y) changes, in terms of standard deviations, when a predictor variable (X_k) changes by one standard deviation. This facilitates the interpretation of the relative influence of each predictor variable on the dependent variable. Note that β_0 is set to zero in standardized models.

We considered the Bayesian Information Criterion (BIC) to select the optimal set of predictors, as it penalizes model complexity and balances explanatory power with parsimony. According to Ghosh et al. (2006), lower BIC values indicate a better model fit, while higher values suggest overfitting or the unnecessary inclusion of variables.

To verify the statistical validity of the fitted models, we tested the main assumptions of multiple linear regression:





- i) Predictors collinearity, assessed through bivariate correlations and the Variance Inflation Factor (VIF; Alin, 2010), VIF values below 3 indicating an absence of significant collinearity.
- ii) Residual independence, tested using the Durbin-Watson test (d; Durbin and Watson, 1951)) for first-order autocorrelation, and the Breusch-Godfrey test (Lm; Breusch and Godfrey, 1986) for higher-order serial correlation.
- iii) Normality of residuals, assessed using the Shapiro-Wilk test (W; Shapiro and Wilk, 1965).
- iv) Homoscedasticity, tested using the Breusch-Pagan test (BP; Breusch and Pagan, 1980).
- v) Influential observations, identified using Cook's distance and hat values to detect outliers affecting model stability (Hoaglin and Welsch, 1978; Cook and Weisberg, 1994; Seheult et al., 1989).

To evaluate the out-of-sample performance of the model, leave-one-out cross-validation (LOOCV; Burman, 1989) was applied. This method fits the model while excluding one observation at a time (in this case, one hydrological year), then the model's predictive performance is assessed using the excluded observation. The process is repeated systematically until all observations have been tested once. This ensures a rigorous assessment of model robustness and generalizability.

Additionally, we considered five case studies for each glacier to separately analyze the effects of climate change, climate variability, and black carbon pollution. These included the following cases: all effects (TE), climate variability (VC), climate change (CC), combined climate effects (CC+VC), and contamination effects (BC), as summarized in Table 4. The models were fitted using different subsets of predictor variables and evaluated using metrics such as the coefficient of determination (R²), root mean square error (RMSE), and mean absolute percentage error (MAPE). This analysis aimed to quantify the explanatory power of each group of variables and their relative importance concerning the observed glacier retreat. The goal was to determine the percentage of glacier retreat explained by each of these causal factors. For the TE and CC+VC cases, we evaluated the effect of the Megadrought by analyzing the role of predictor variables in glacier area changes during the pre-megadrought (2000–2009) and post-megadrought (2010–2020) periods.

For each MRLM in the TE, VC, CC, CC+VC, and BC cases, model performance—both during model fitting and validation—was evaluated using these statistical metrics. All statistical tests were conducted at a significance level of 5%.

Table 4. Case studies representing climatic and contamination effects on the retreat of POG and BG.

Case Studies	Abbreviation	Analized variables
All effects	TE	DTbCero, Precipitation, Niño 3.4, PDO, and BC
Climate variability	VC	Niño 3.4 and PDO
Climate change	CC	DTbCero and Precipitation
Climate Effects	CC+VC	DTbCero, Precipitation, Niño 3.4, and PDO
Contamination effects	BC	ВС



255

260

265



250 3 Results and Discussion

3.1 Detection of Glacier Area

Figures 3a and 3b show the variation in surface area of the POG and BG glaciers, respectively, from the 2000 to the 2020 hydrological year, based on one Landsat image per summer. Both glaciers have experienced a significant reduction in surface area, especially in their mid- and low-elevation zones (Figure 3a,b). For POG, the northwestern tongue has completely disappeared, and a glacial lake has begun to form in the southwestern sector (Figure 3a). In contrast, BG shows more pronounced shrinkage on its eastern side, primarily because that slope faces northwest and thus receives greater solar radiation during the summer months (Figure 3b). Figure 3c shows the percentage of glacier surface reduction relative to the first evaluation year (2000). As observed in Figures 3a and 3c for POG, the glacier area has steadily decreased over the study period, reaching up to a 45% loss in the last two years of the study, with an ablation rate that has doubled since 2010 (Figure 3d). BG, while also diminishing over time, has maintained an ablation rate about one-quarter of that observed for POG (Figure 3c). Notably, POG even showed slight area increases between 2004 and 2007 (Figure 3d), possibly due to climatic factors, such as the marked La Niña event in 2007, which brought heavy snowfall to central Chile and freezing levels as low as 560 meters above sea level during winter (Vicencio et al., 2017). Another example occurred in 2005, when annual accumulated precipitation reached its highest value between 2000 and 2020 (Figure 3a).

Figure 3d presents the time series of glacier area (in km²) and ablation rates over time. In year 2000, POG covered an area of 1.33 km², declining to 0.77 km² in 2020, with an average annual reduction rate of 2.1% per year. BG, which extended for 4.21 km² in 2000, decreased to 3.61 km² by 2020, at a rate of 0.7% per year. A distinct inflection point in the glacier area time series is observed between 2009 and 2010 (Pettitt Test, PT), which coincided with an increase in ablation rates for both glaciers, an effect linked to the onset of the Megadrought (Garreaud et al., 2017). During the period 2000–2010, the ablation rates were -0.28 km² per decade for POG and -0.30 km² per decade for BG. However, during the Megadrought, these rates intensified, reaching -0.35 km² per decade for POG and -0.60 km² per decade for BG. In all cases, the trends are negative and statistically significant (p-value < 0.05) for both glaciers. At the current rate of retreat, POG could disappear in just over 10 years.

3.2 Exploratory Data Analysis

Figure 4 shows the annual accumulated precipitation, the number of days with temperatures below 0°C (DTbCero), macroclimatic indices, and BC concentration deposited on snow for each hydrological year during the study period at both glaciers. Each pannel includes results from the Mann-Kendall (MK) and Pettitt (PT) tests, as well as Pearson correlations, indicating significant trends (p-value < 0.05), the year of any detected shifts, and correlations between series, respectively. For the macroclimatic indices, no statistical tests were applied, as these indices primarily represent oscillations around mean sea surface temperatures and are expected to exhibit cyclical rather than linear trends.

Figure 4a reveals a significant negative trend in annual precipitation for both glaciers, with declines of approximately -286 mm per decade for POG and -293 mm per decade for BG. The PT tests indicate a regime shift around 2010, after which





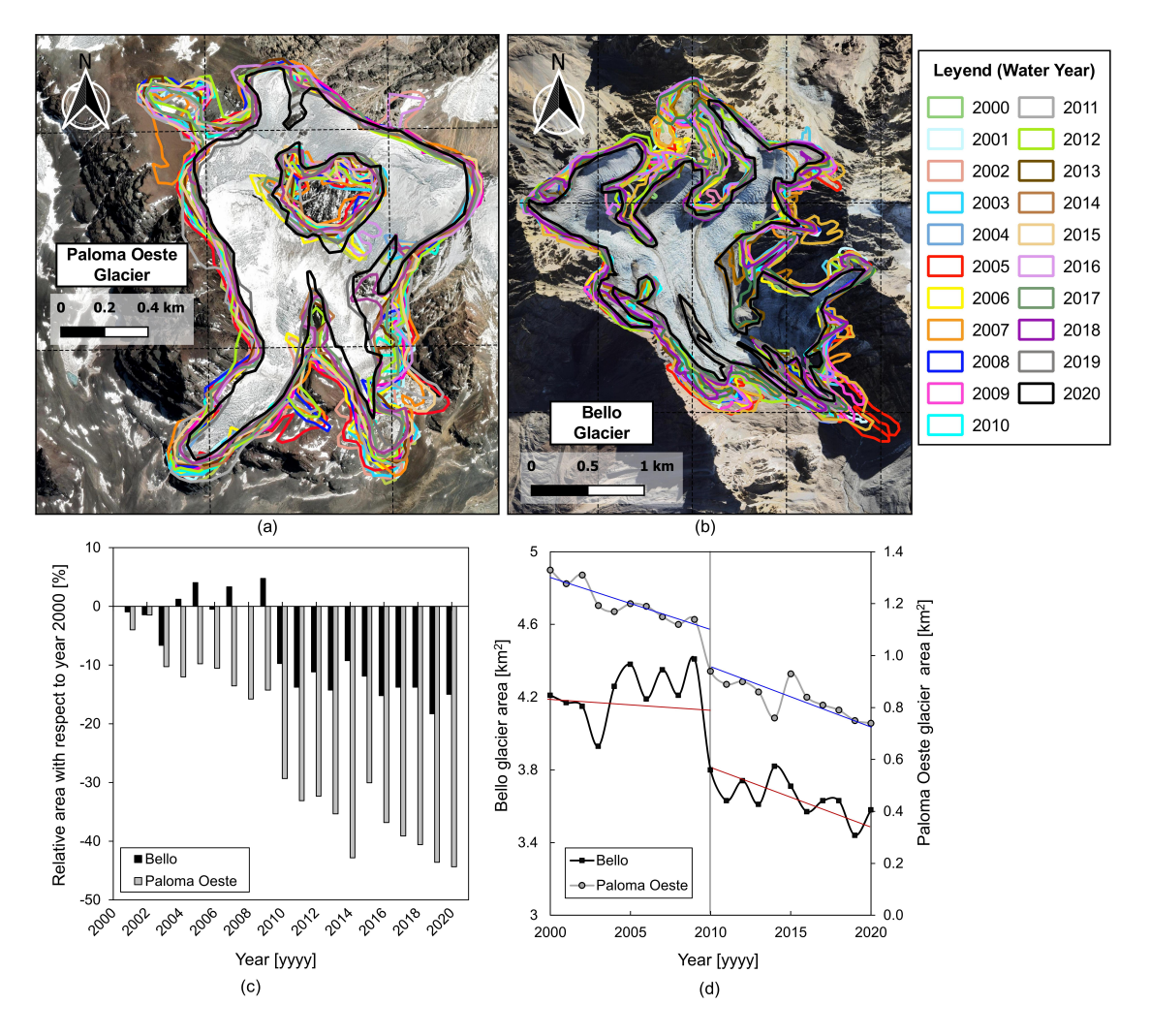


Figure 3. Spatial and temporal variation in glacier surface area between the 2000 and 2020 hydrological years, obtained from Landsat imagery. (a) Paloma Oeste Glacier and (b) Bello Glacier, showing annual glacier boundaries. (c) Changes in glacier area relative to the year 2000 for both glaciers. (d) Glacier area changes over time, highlighting the trend shift associated with the onset of the Megadrought around 2010.

the negative trend intensified, reaching approximately -430 mm per decade for POG and -460 mm per decade for BG. The precipitation series for POG and BG are strongly correlated (r = 0.86), consistent with their shared climatic zone and similar mid-elevation ranges. Similarly, Figure 4b shows a significant decreasing trend in the number of days with temperatures below 0°C, with reductions of about -12 days per decade for POG and -14 days per decade for BG. The PT tests identify 2011 as the year of inflection for both glaciers, after which the decline steepened to approximately -17 days per decade. Both the precipitation and DTbCero series exhibit marked changes coinciding with the onset of the Chilean Megadrought, highlighting significant shifts in local climate dynamics during the last decade.



295

300

305



Figure 4c presents shows the macroclimatic indices over the study period. In recent years, the PDO has predominantly remained in negative phases, which may contribute to cooler conditions and a decrease in precipitation in central Chile, as previously discussed (Garreaud et al., 2009; Núñez et al., 2013). Notably, although the Niño 3.4 index showed an intense positive phase in 2015, indicating a marked El Niño event, this was not reflected in the snowfall that year, suggesting that large-scale climatic anomalies do not always translate directly into local hydrological responses. Figure 4d shows the BC concentration on the glacier surface, derived from CAMS data, with a multi-year average of 28 $\mu g \cdot cm^2$ for POG, which is about 40 times higher than the mean value for BG (0.7 $\mu g \cdot cm^2$), indicating a substantial difference in pollution exposure between the two sites. Moreover, BC concentration in POG exhibits significant interannual variability and a rising temporal trend, with the highest values observed since 2015. The MK test applied to the annual BC time series revealed a significant positive trend (p-value < 0.05) for POG, at a rate of +0.41 $\mu g \cdot cm^2 \cdot yr^{-1}$, whereas BC levels in BG did not show a significant trend (p-value > 0.05), showing only a slight increase of +0.004 $\mu g \cdot cm^2 \cdot yr^{-1}$.

For each glacier, we calculated correlations between the time series of potential drivers of glacier retreat and the glacier area series. Table 5 presents the Pearson correlation coefficients for all potential predictor variables and glacier area. A strong negative correlation was observed between glacier area and BC concentration for both POG and BG (r > 0.7). High correlations were also found with precipitation and DTbCero, while Niño 3.4 showed a high correlation with glacier area for BG and a moderate correlation for POG. In contrast, the PDO exhibited moderate correlations in both glaciers. Furthermore, no high correlations (r < 0.6) were identified among the predictor variables themselves, suggesting low multicollinearity and supporting the suitability of these variables for inclusion in the MRLM.

Table 5. Pearson correlation coefficients among time series of glacier area and climatic, macroclimatic, and pollution variables for BG and POG.

POG	Area	Temperature	Precipitation	Niño 3.4	PDO	Black Carbon	
BG	[Km2]	[days]	[mm]	[-]	[-]	[ug/cm2]	
Area		0.628**	0.764***	0.612**	-0.617**	-0.815***	
Temperature	0.719***		0.498*	-0.220	-0.294	-0.489*	
Precipitation	0.630**	0.484*		0.336	-0.148	-0.583*	
Niño 3.4	0.685***	-0.211	-0.301		0.466*	0.227	
PDO	-0.592**	-0.324	-0.133	0.466*		0.239	
Black Carbon	-0.694***	-0.413*	-0.335	0.234	0.172		
(***) High Correlation (**) Moderate Correlation (*) Low Correlation							
	Pearson cor	relation for BG		Pears	on correlation	on for POG	

3.3 Best MLRM Selection and Adequacy Verification

After ruling out high correlations among predictor variables, selecting appropriate regressors for the MRLM is essential. The BIC provides a relative measure of model quality and facilitates the exclusion of statistically insignificant independent variables





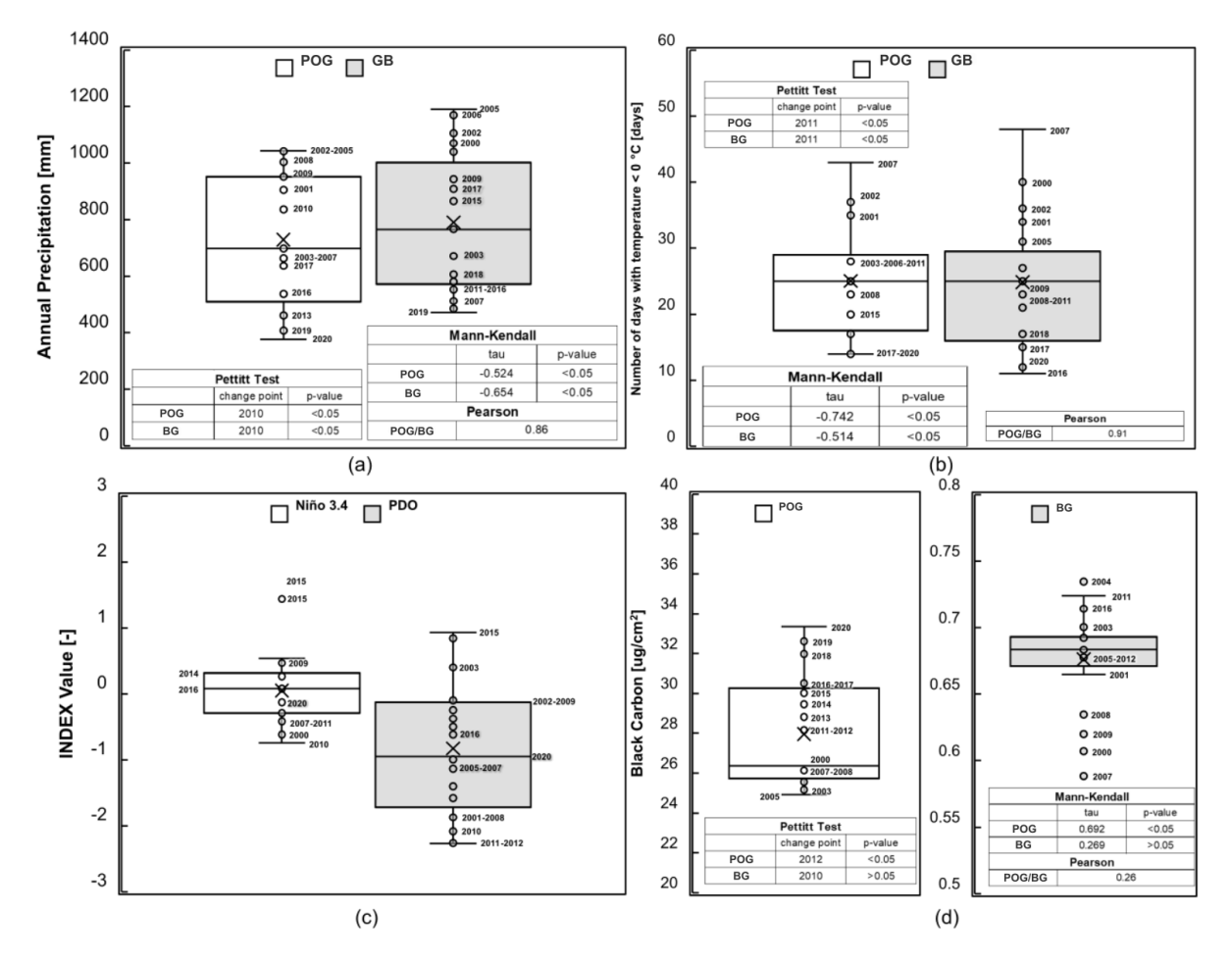


Figure 4. Annual time series of the variables included in the regression model, together with results from the Mann-Kendall test, Pettitt test, and Pearson correlation between the time series of POG and BG. (a) Accumulated precipitation (2000–2020). (b) DTbCero. (c) Macroclimatic indices: Niño 3.4 (May–September average) and PDO (August–October average). (d) BC concentration on snow for POG and BG, expressed in $\mu g \cdot cm^2$.

(p-value > 0.05). Figure 5 shows the BIC values for the regression models, indicating that the best fit for both glaciers is achieved when combining climatic variability (macroclimatic indices), climate change indicators (precipitation and DTbCero), and BC pollution. The second-best fit in both glaciers is obtained when excluding the DTbCero variable, suggesting that it has a lower influence on glacier area variation compared to other predictors; however, this is not the case for precipitation, which consistently appears among the top three models and is considered necessary due to its role in balancing glacier ablation (McCarthy et al., 2022). Furthermore, when considering models with a single predictor, the best-fitting model for POG is obtained using only BC, whereas for BG, the best-fitting model results from using only the DTbCero variable (climate change).

Table 6 summarizes the statistical test results used to verify the assumptions of the MRLMs fitted for the TE case. We evaluated the following conditions: absence of collinearity among predictors, as well as normality, homoscedasticity, and



335

340



temporal independence of the residuals. Additionally, an analysis of influential values was performed to identify years with a disproportionate impact on the models. While we had already checked for collinearity through the bivariate correlation analysis (Table 5), this was further confirmed by calculating the Variance Inflation Factor (VIF). All predictors showed VIF values below 3, indicating low intercorrelations among predictors and, consequently, no evidence of significant collinearity. The residual analysis shows that, for both models, the errors follow a normal distribution (Shapiro–Wilk test), exhibit homoscedasticity (Breusch–Pagan test), and do not exhibit temporal autocorrelation (Durbin–Watson and Breusch–Godfrey tests). These results confirm that the fundamental assumptions underlying the validity of the MRLMs are satisfied.

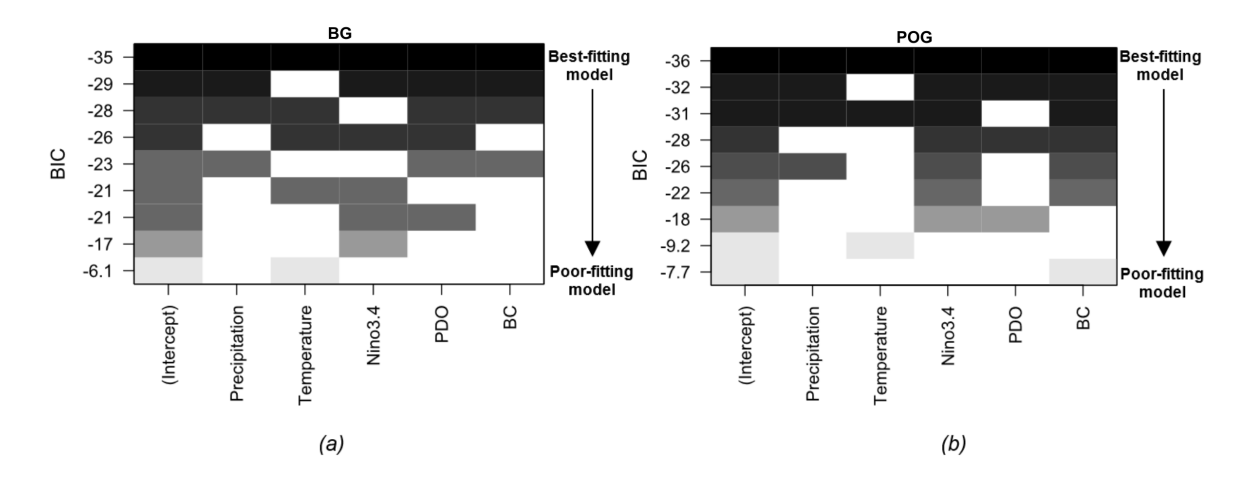


Figure 5. BIC values for selecting predictor variables to model glacier area change in an MRLM. (a) BG. (b) POG.

In the analysis of influential values, both glaciers show two coincident years with a high statistical influence: 2007 and 2015. The year 2007 was characterized by unusually low temperatures and heavy snowfall at low elevations in central Chile, which may have significantly affected glacier retreat. In 2015, a strong El Niño event occurred, with an average Niño 3.4 index of +2.3 °C. However, unlike other similar events, that year was anomalously dry, which may help explain its influence on the models. Notably, according to Figure 4, 2015 was also one of the five years with the highest BC concentrations in POG, further supporting its potential role in glacier dynamics. In contrast, in BG, the year 2007—also identified as influential—recorded the lowest BC concentration of the study period, suggesting that its influence is mainly due to exceptional climatic conditions rather than BC pollution. For POG, the years 2002 and 2005 were also identified as influential, both of which were associated with precipitation significantly exceeding historical averages; for instance, in 2002, it surpassed the period mean by a notable margin. In the case of BG, 2006 was identified as influential, while 2016 stood out as the year with the fewest days below freezing in the entire series, reflecting exceptionally warm conditions. The analysis of these years helps identify relevant climatic anomalies that disproportionately influence model outcomes, making their identification essential for interpreting the processes driving glacier retreat.

Figure 6 presents a comparison between the glacier area simulated by the MRLMs and the values observed from satellite imagery. A strong linear relationship is observed between the two series, with coefficients of determination (R^2) of 0.985 for





BG and 0.975 for POG, indicating that the models explain more than 95% of the observed variability and thus validate their predictive capability.

Table 6. Statistical tests to validate the assumptions of the MRLMs. The test statistic, p-value, and the assumption being tested are presented. The significance level of the tests is 0.05

			POG				BG	
Test	Test Statistic		P-value	Conclusion	Test Statistic		P-value	Conclusion
Durbin-Watson	d: 1.707		0.860	No correlation between the residuals (Linear)	d: 2.010		0.341	No correlation between the residuals (Linear)
Breush-Godfrey	Lm: 1.843		0.123	No correlation between the residuals (Nonlinear)	Lm: 2.422		0.094	No correlation between the residuals (No linear)
Shapiro	W: 0.9663		0.650	The residuals follow a normal distribution	W: 0.9548		0.418	The residuals follow a normal distribution
Breusch-Pagan	BP: 7.4228		0.191	Residual variance is constant (Homoscedasticity)	BP: 3.7733		0.583	Residual variance is constant (Homoscedasticity)
Analysis		Values	3	Conclusion		Values	3	Conclusion
	Niño 3.4:		1.331		Niño 3.4:		1.626	
	PDO:		1.631	There is no	PDO:		1.632	There is no
VIF Test	Precipitation:		1.609	collinearity	Precipitation:		1.514	collinearity
	Temperature:		1.267	(VIF <3)	Temperature:		1.479	(VIF <3)
	BC:		1.906		BC:		1.463	
		Hat	Cook's distance			Hat	Cook's distance	
	2005	1.294	2.565	36 6	2016	0.876	1.134	N
Influence analysis	2007	1.125	2.126	Most influential	2007	1.135	2.823	Most influential
	2015	1.359	2.892	years:	2006	0.914	1.729	years:
	2002	0.934	1.245	2004 and 2015	2015	0.995	2.118	2007 and 2015

3.4 Cross-validation

To validate the previously fitted models for each glacier, we used the LOOCV method. Figures 7a and 7b show scatter plots of observed versus estimated glacier area values obtained from the MRLMs under LOOCV for different predictor combinations, and each graph is accompanied by goodness-of-fit metrics, including R², MAPE, and RMSE, for POG and BG, respectively. Both models exhibit high R² values, indicating that they account for a substantial proportion of the variance in the observed data around their means. Additionally, the RMSE is less than 0.1 km² in both cases, and the MAPE remains below 0.1%. However, predictions deviate from actual values in some years; for example, in 2015, exceptional circumstances affected climatic conditions, and consequently, the behavior of glacier areas. Figures 7c and 7d, show the residuals of the models fitted using total effects (TE), indicating residuals below 5% in both glaciers, with lower residuals observed in BG compared to POG. Overall, the predictor variables included in the models adequately capture the variability in the data.





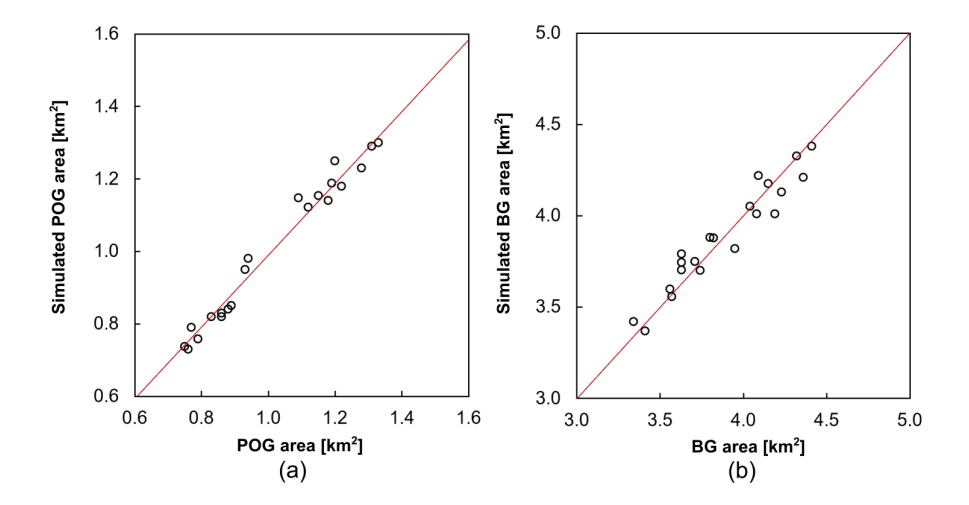


Figure 6. Glacier area simulated by MRLMs versus observed values (non-standardized). (a) BG. (b) POG.

3.5 Sensitivity Analysis

Table 7 presents both standardized and unstandardized coefficients obtained from the regression models fitted for each glacier. Standardized coefficients allow comparison among the variables analyzed, as they eliminate differences in predictor magnitudes. However, while standardized coefficients indicate the sensitivity of each variable to glacier area, the magnitude of the drivers of retreat varies from year to year, depending on conditions such as wetter years, more frequent cold days, marked El Niño events, and/or varying BC concentrations. Therefore, changes in glacier area are analyzed using both types of coefficients.

The standardized coefficients shown in Table 7 reveal a positive sensitivity of glacier area to DTbCero, annual accumulated precipitation, and the Niño 3.4 index from May to October. The opposite occurs with PDO and BC; while the negative effect of BC on glacier area is expected due to greater radiative forcing and accelerated melting, the sign of the PDO coefficient was unexpected and suggests a more complex or indirect influence on glacier dynamics. The glacier area in both glaciers shows greater sensitivity to the Niño 3.4 index (positive) and BC concentration (negative) than to precipitation, PDO, and DTbCero.

Furthermore, for both BG and POG, glacier retreat exhibits less sensitivity to DTbCero compared to the PDO index and annual accumulated precipitation.

Table 7. Regression coefficients and standardized coefficients estimated from the MRLMs fitted for POG and BG.

	DTbCero	Precipitation	Niño 3.4	PDO	BC	Intercept
		Regression	coefficients /standa	ardized coefficients		
POG	0.0048/0.2370*	0.0004/0.2735*	0.0510/0.3093*	-0.0367/-0.2664*	-0.0602/-0.2851*	1.2399/0*
BG	0.0112/ 0.2255*	0.0007/0.2293*	0.1983 /0.3733*	-0.0768/-0.2284*	-0.9136/-0.3249*	3.8610/0*



375



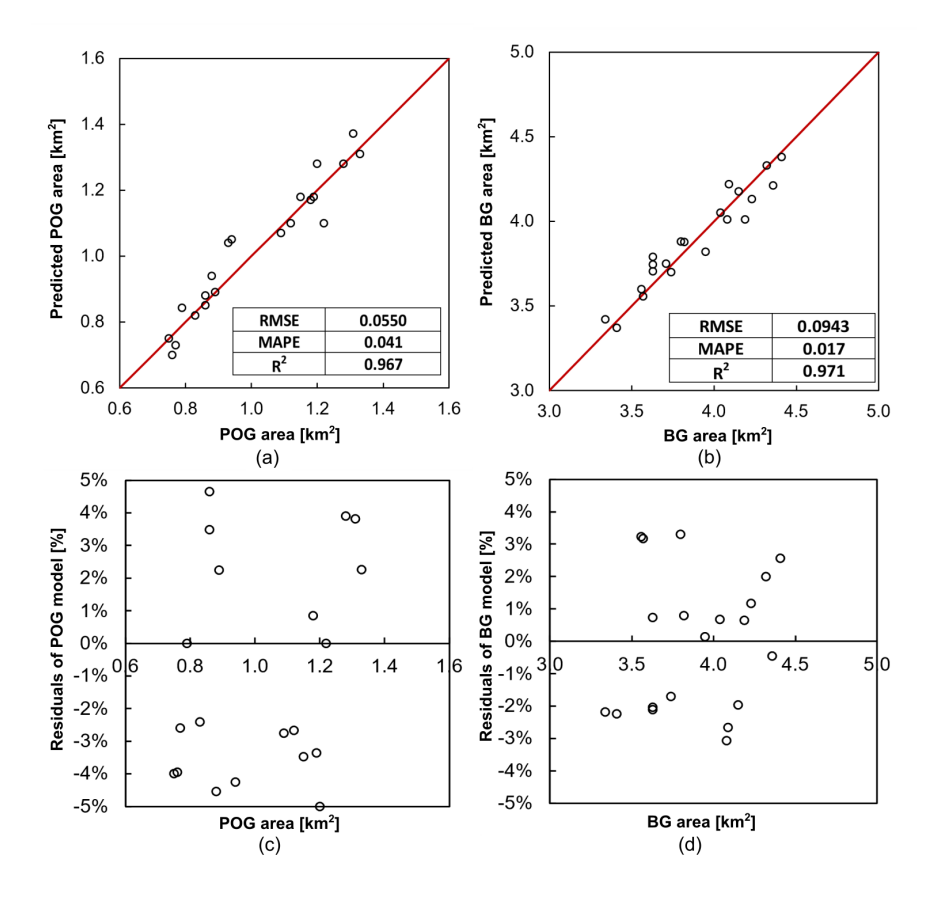


Figure 7. R², MAPE, and RMSE values obtained through LOOCV validation applied year by year for (a) POG and (b) BG. In addition, residuals of the regression model adjusted using all effects (TE) are shown for (c) POG and (d) BG.

It is important to highlight that both models show sensitivity of glacier area to BC pollution, underscoring the significant role of this contaminant in glacier melt that helps explain the faster retreat observed in POG compared to BG. As shown in Figure 1, POG is located near a major pollution source associated with mining operations. Our findings align with the results of Masiokas et al. (2020) and Chinn et al. (2005), who emphasized the role of precipitation and the El Niño phenomenon in influencing glacier dynamics in the Central Andes, as well as in other mountain regions worldwide. Furthermore, the sensitivity analysis using the standardized model suggests that a hypothetical increase in BC concentration could have a more severe impact on glacier retreat than an equivalent decrease in winter temperatures. Although the model was not designed for predictive purposes, these results help identify which factors may carry greater relative weight in future glacier evolution under environmental changes, reinforcing the need to mitigate local pollution sources.

To evaluate glacier area variations between consecutive years ($year_i$ - $year_{i-1}$), unstandardized MRLMs were used. This approach aims to determine the portion of each yearly variation attributable to each predictor (Figure 8). For each period ($year_i$ - $year_{i-1}$), the sum of area changes attributable to each predictor was calculated, with the total sum matching the overall



380

385

390

395

400

405

410



area variation between the two years analyzed. The analysis began with the 2001-2000 period and continued to assess the contributions of each predictor variable over the last 20 years for both glaciers. Figure 8 shows both positive and negative variations in glacier area throughout the study period, driven by fluctuations in DTbCero, annual accumulated precipitation, macroclimatic indices, and BC time series for both glaciers. At the top of each graph, a table summarizes the cumulative glacier area changes attributable to each predictor. The total sum of these variations corresponds to the overall glacier area change between 2000 and 2020, as estimated by the fitted models, amounting to -0.58 km² for POG and -0.62 km² for BG. In most years, BC led to negative changes between consecutive periods, contributing a total area variation of -0.28 km² for POG and $-0.02~\mathrm{km^2}$ for BG. The next most significant factor was accumulated precipitation, with total area changes of $-0.17~\mathrm{km^2}$ for POG and -0.21 km² for BG. Although positive variations occurred during wetter years, overall, glacier area decreased in most years of the megadrought period after 2010. DTbCero emerges as an important driver of glacier area variation for both glaciers, contributing a total area change of -0.37 km² in BG and -0.12 km² in POG. Regarding the Niño 3.4 and PDO, their contributions—whether positive or negative—to glacier area changes are similar in both glaciers and account for less than 10% of the contribution from DTbCero or annual accumulated precipitation. Moreover, after 2010, surface variations attributable to changes in the PDO and Niño 3.4 indicators intensified compared to those observed before 2010. For example, in POG, Niño 3.4's contribution shifted from approximately 0.0 km^2 before 2010 to -0.45 km^2 after 2010, and PDO from around -0.02 km^2 to -0.11 km^2 ; in BG, Niño 3.4 went from about 0.02 km^2 to -0.28 km^2 , and PDO from -0.02 km^2 to -0.10 km^2 .

When analyzing the results by annual intervals, wet years such as 2004–2005 and 2007–2008 were identified, during which precipitation was the dominant variable associated with increased glacier surface area in both glaciers (Figure 8). In contrast, during the 2007 hydrological year, which was marked by unusually low temperatures, DTbCero emerged as the decisive variable in the 2006–2007 and 2007–2008 intervals, although with opposite effects in each glacier. The 2015–2016 interval marked one of the greatest area losses, coinciding with a high number of sub-zero days (DTbCero). However, this retreat was primarily attributed to the Niño 3.4 index, which was associated with a significant deficit in solid precipitation that year (Escobar and Aceituno, 1998; Masiokas et al., 2006), along with the PDO index, which has been linked to higher spring temperatures (Mendez et al., 2011), thus favoring ice melt.

Figure 8 also shows the percentage of glacier area loss attributable to climatic effects (DTbCero, precipitation, PDO, and Niño 3.4) and pollution (BC). This calculation was performed by adding the area variations attributed to climatic drivers (DTbCero + precipitation + PDO + Niño 3.4) or pollution (BC) and then determining their percentage contribution relative to the total glacier area change between 2000 and 2020. Here, DTbCero and precipitation represent climate change (CC), while the PDO and Niño 3.4 indices reflect climate variability (CV). The results indicate that for POG, 49% of glacier retreat was due to pollution (BC), while 51% resulted from climatic effects (CC + CV). In contrast, for BG, 97% of the retreat was attributed to the climatic effects, and only 3% to BC pollution.

The interannual variation in the magnitude of climatic and pollution variables between 2000 and 2020 helps explain why certain predictors exerted greater influence in specific years. This differential behavior is clearly reflected in the unstandardized models, where absolute contributions to glacier retreat vary significantly between intervals and between glaciers. For POG, the greatest retreat occurred during years with high BC concentrations, whereas in BG, retreat was mainly associated with thermal





conditions (DTbCero) and low precipitation. This contrast in dominant drivers is explained by the substantial disparity in BC concentrations between the glaciers: in POG, BC levels were more than 40 times higher than those in BG. This suggests that pollution has played only a marginal role in BG's retreat over the last two decades, in contrast to its significant influence on POG. Since both glaciers share similar climatic and geomorphological conditions, this difference reinforces the hypothesis that proximity to emission sources is a critical factor in glacier retreat dynamics.

In line with these findings, Cereceda-Balic et al. (2022) compared BG with Olivares Alfa Glacier—located near POG—and estimated that 82% of Olivares Alfa's retreat between 2004 and 2014 was attributable to BC pollution. Consistently, the present study determined that between 2000 and 2020, 49% of POG's glacier retreat was due to BC pollution and 51% to climatic factors (CC + CV), whereas for BG, with very low exposure to BC, 97% of the retreat was attributed to climatic causes and only 3% to pollution.

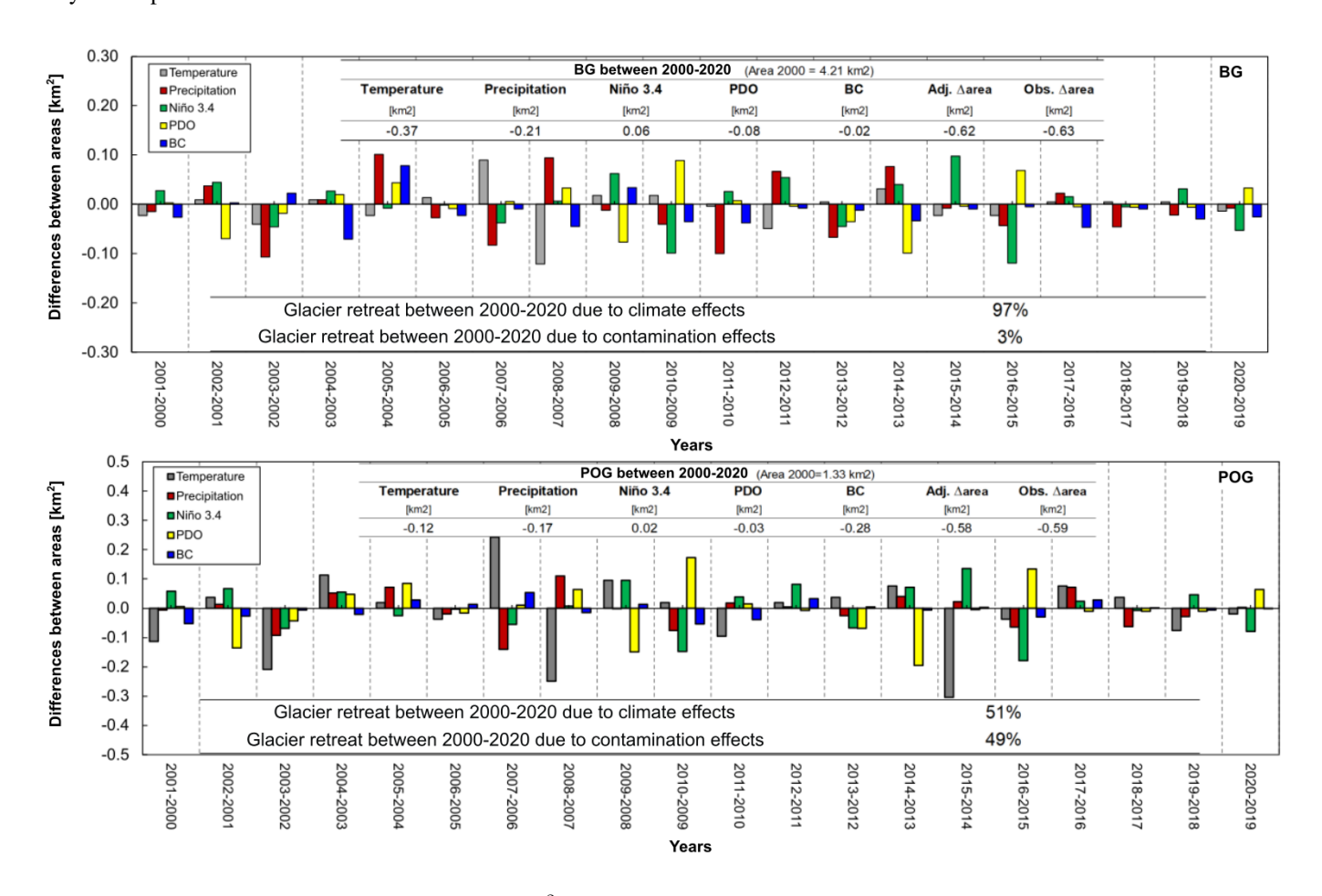


Figure 8. Glacier area changes for POG and BG (in km²) between consecutive years, estimated from unstandardized coefficients of the MRLMs for each predictor. The upper table summarizes the cumulative area changes attributed to each predictor and the total glacier area variation between 2000 and 2020. The lower section of each figure shows the percentage contribution of climatic effects and pollution (BC) to the overall glacier area change.



435

440



Figure 9 shows the regression parameter values for the different case studies described in Table 4, evaluating various potential drivers of glacier retreat, including climate change (CC), climate variability (CV), their combined climatic effects (CC+CV), Black Carbon pollution (BC), and the combined influence of all variables (TE). As expected, the TE case yields the highest R² and KGE values and the lowest RMSE and MAPE values, indicating good model fit and the ability to capture temporal variability, bias, and variance. Furthermore, the best-performing model differs between glaciers. For BG, the best fit was achieved with the CC+CV model. In contrast, for POG, the complete set of predictors was necessary to achieve a good fit, as each subset explained only part of the variance, resulting in higher estimation errors. Interestingly, a model using only BC as a predictor performs substantially better for POG than for BG. In BG, however, BC as a sole predictor results in considerable error, unlike in POG. This finding further supports earlier conclusions about the significant role of BC in POG compared to BG. Overall, in both glaciers, climatic effects as a whole (CC + CV) play an essential role in explaining glacier area changes and should be considered jointly. Moreover, when climate change and climate variability are analyzed separately, the goodness-of-fit parameters are similar for both glaciers, as both ice bodies are located within the same climatic zone.

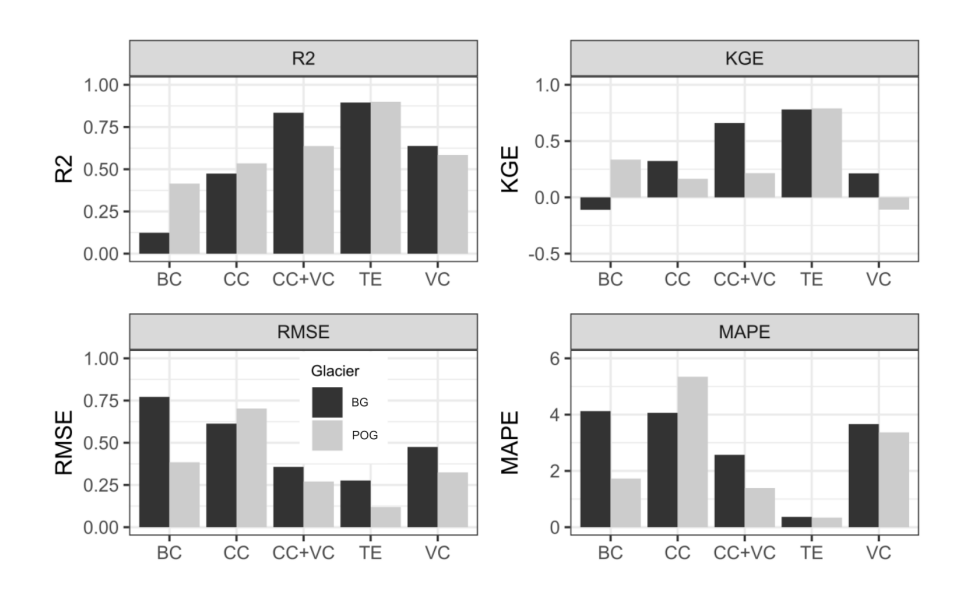


Figure 9. Goodness-of-fit metrics (R², KGE, RMSE, and MAPE) for regression models fitted using the variables included in each case study (BC, CC, CC+CV, CV, and TE), with results shown separately for BG and POG.

3.6 Impact of the Megadrought on Glacier Retreat Dynamics

To determine the influence of the Megadrought period on glacier retreat, we analyzed potential trend changes in the residuals from the regression models fitted for each case study (TE, CC, CV, BC, and CC+CV; see Table 4). For this purpose, we applied the Pettitt test to the residual series of each model. Table 8 displays the results, revealing significant trend shifts only in the models representing climate change (CC) and combined climatic effects (CC+CV). In both glaciers, the detected shift





occurred in 2010, coinciding with the onset of the Megadrought—a persistent dry period documented by Garreaud et al. (2017) as a transition from predominantly wet conditions during the 20th century to sustained reductions in precipitation and progressively increasing temperatures, severely impacting the region's hydrological balance. This climatic shift is reflected not only in regional meteorological variables such as precipitation and DTbCero but also in glacier dynamics. Residuals from the CC+CV models for both POG and BG exhibited a clear breakpoint around 2010, indicating a shift in glacier retreat patterns.

Table 8. Results of the Pettitt test for trend changes in residuals of MRLMs fitted for different case studies in POG and BG.

	POG		BG			
Case study	Pettitt Test P-value	Change Point	Case study	Pettitt Test P-value	Change Point	
TE	0.82	_	TE	0.89	_	
CC	0.03	2010	CC	0.04	2010	
VC	0.25	_	VC	0.16	_	
CC+VC	0.04	2010	CC+VC	0.05	2010	
BC	0.81	-	BC	0.75	_	

Further evidence of this shift comes from the analysis of the root mean square error (RMSE) values for the MRLMs across both periods (Figure 10a). In BG, the RMSE decreased after 2010, suggesting that its retreat became more consistently explained by climatic conditions. In contrast, POG's RMSE increased in the same period, reflecting greater complexity in its dynamics, likely due to interactions between climatic drivers and persistently high BC levels.

Figure 10b further illustrates glacier retreat driven by climatic drivers (CC+CV) and pollution effects (BC) before and after 2010. Before 2010, climatic effects accounted for 47% of glacier retreat in POG and 94% in BG. After 2010, these contributions rose to 61% for POG and 97% for BG, highlighting an increased role of climate in glacier retreat during the Megadrought period. Conversely, the contribution of BC to retreat in POG decreased from 53% before 2010 to 39% after 2010, suggesting that although BC remains a significant factor for POG, climatic drivers became more dominant during the Megadrought. For BG, the contribution of BC declined modestly from 6% to 3%, underscoring that glacier retreat in the area has remained overwhelmingly driven by climatic factors.

These findings align with Farías-Barahona et al. (2020), who reported that shifts in precipitation and temperature patterns during the Megadrought were correlated with accelerated glacier retreat in the central-southern Andes. Our results similarly indicate that, after 2010, climatic effects emerged as the primary driver of glacier retreat in the study region, even for glaciers with substantial exposure to pollutants, such as POG. Overall, these findings reinforce the conclusion that since the onset of the Central Chile Megadrought, climatic conditions have become the dominant force behind glacier retreat in Central Chile, even in glaciers where black carbon pollution continues to exert a significant influence.





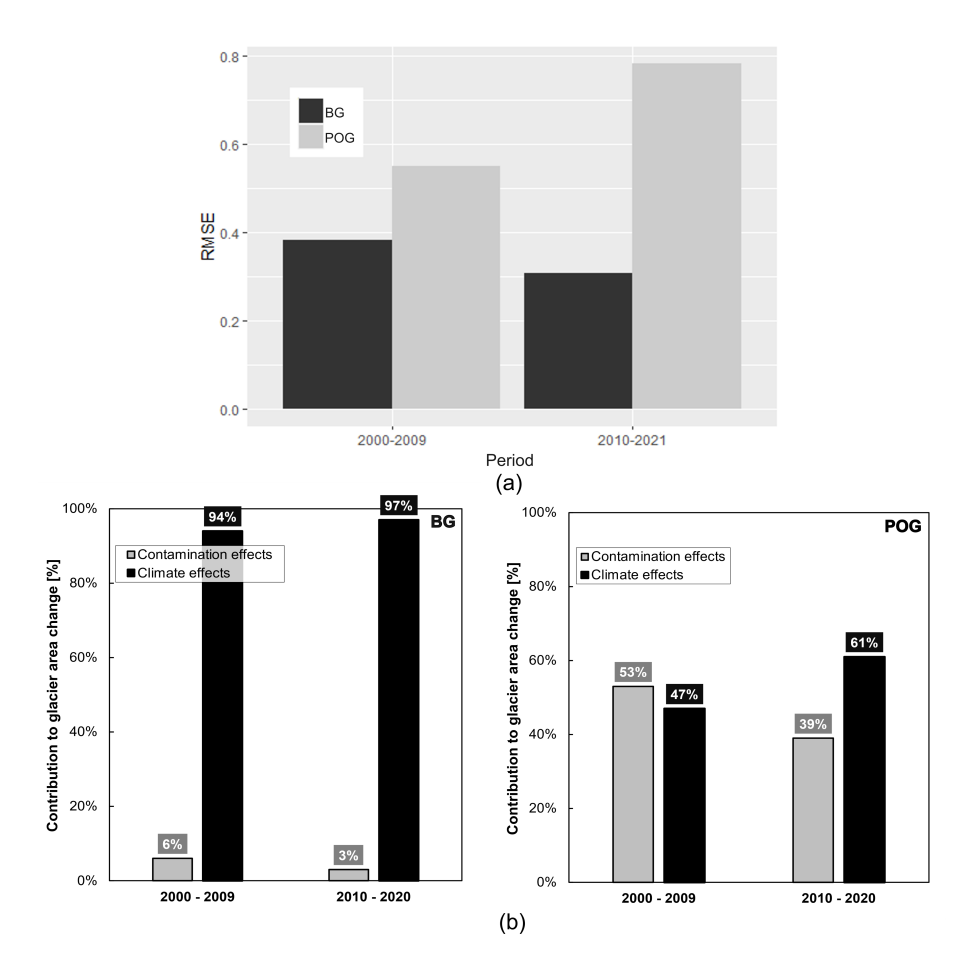


Figure 10. Megadrought effects on glacier retreat. Glacier retreat of each ice body between 2000–2009 and 2010–2020, estimated from unstandardized regression models and quantifying the proportion of retreat attributed to each analyzed cause. The figure shows the percentage of glacier retreat driven by climatic effects (CV+CC) and by pollution effects (BC).

4 Conclusions

465

470

In this study, two glaciers located in the Maipo River Basin—Paloma Oeste Glacier (POG) and Bello Glacier (BG)—were analyzed. Although these glaciers share similar climatic and geomorphological settings, they differ in contamination levels and retreat rates. To investigate the factors driving their retreat, multivariable regression models (MRLMs) were developed for each glacier, incorporating variables linked to climate change (CC), climate variability (CV), and pollution (BC).

The analyses revealed a significant temporal shift around 2010, coinciding with the onset of the Megadrought. Before this period, glacier retreat rates were $-0.28~\mathrm{km^2}$ per decade for POG and $-0.30~\mathrm{km^2}$ for BG. During the Megadrought, retreat rates increased significantly (p-value < 0.05) to $-0.60~\mathrm{km^2}$ and $-0.35~\mathrm{km^2}$ per decade, respectively. Climatic variables such as hydrological year precipitation and DTbCero (days with temperatures below $0^{\circ}\mathrm{C}$) also exhibited marked changes after 2010. In



485

495

500



POG, precipitation decreased from -286 mm to -430 mm per decade, while in BG it declined from -293 mm to -460 mm per decade. DTbCero decreased more sharply as well, shifting from an average of -13 days to -17 days per decade in both glaciers. Regarding pollution, BC deposited on snow did not vary significantly between periods. However, a pronounced difference lies in its magnitude: BC concentrations in POG are 40 times higher than those in BG, with significant positive trends observed in POG over the study period, whereas trends in BG were not significant. This notable difference suggests that local pollution plays a pivotal role in POG's retreat.

The MRLMs effectively identified variables contributing to glacier area changes. Using the Bayesian Information Criterion (BIC), the selected predictors included both climatic variables (CV+CC) and BC. The models were tested for collinearity 480 and met assumptions of residual normality, independence, and homoscedasticity. Cross-validation confirmed the robustness of the models, with residuals below 5% in all cases, and the MRLMs explained over 95% of observed glacier area variability. Analysis of standardized coefficients revealed that glacier area in both glaciers responded positively to DTbCero, accumulated precipitation, and the Niño 3.4 index, and negatively to PDO and BC. BC consistently showed higher standardized coefficients compared to other predictors, underscoring its significant impact on glacier melt, particularly in POG. Unstandardized coefficients were further used to quantify glacier area changes between consecutive years, highlighting the drivers behind interannual variability. This analysis revealed that for POG, 49% of the variation was attributed to BC, and 51% to climatic factors (CC+CV), whereas in BG, only 3% was explained by BC, and 97% by CC+CV. These differences account for the divergent retreat rates observed between the two glaciers. Notably, in POG, the recent accelerated retreat is closely associated with BC pollution, which is linked to two nearby mining operations located less than 10 km away.

490 The Megadrought's impact was evident in the MRLM results, as only models incorporating climatic variables showed significant shifts (Pettitt analysis) at the beginning of the event. After 2010, accumulated precipitation and DTbCero changed markedly, with trends from the prior period intensifying—precipitation decreasing significantly and DTbCero increasing—thereby amplifying glacier retreat rates. Sensitivity analyses confirmed that glacier area variation increased during the Megadrought, driven primarily by climatic factors. Nonetheless, approximately 39% of the variation in POG remains influenced by BC, emphasizing the dual impact of climate and local pollution on glacier dynamics.

Currently, measurements of BC deposition are sparse and geographically limited across the Chilean Andes, with no continuous long-term records. Existing data are spatially localized and have only recently begun to be collected (Cereceda-Balic et al., 2019; Cordero et al., 2022). This scarcity of data underscores the need to expand field-based measurements of BC to enhance model calibration and improve understanding of pollution impacts. Understanding the drivers of glacier retreat in Central Chile is critical, given the region's reliance on glacier meltwater for summer water supplies. This study demonstrates the significant influence of climate change on glacier retreat in the Andes. However, in glaciers such as POG, local pollution—particularly BC—also plays a crucial role. These results underscore the need to integrate both climatic and pollution factors into glacier monitoring, modeling, and management strategies in Central Chile.

Data availability. Data provided on request.





Author contributions. The idea and setup for the paper were jointly developed by the five co-authors. The model implementation and analysis were performed by KV and discussed with the co-authors. KV wrote the first draft of the manuscript, which was revised and edited by LC, AO, RF, and FM.

Competing interests. The contact author has declared that none of the authors has any competing interests.

Acknowledgements. This research was funded by Proyecto de Investigación Multidisciplinaria, code PI_M_24_03 from the Universidad

510 Técnica Federico Santa María.LC was sopported by ANID FONDECYT iniciación 11220482. AO was supported by ANID FONDECYT

Iniciación 11250238. RF was supported by ANID FONDECYT 1231494.

During the preparation of this work the author(s) used ChatGPT, Geminai and Deepseek in order to improve the readability and language of the manuscript. After using this tool/service, the authors reviewed and edited the content as needed and took full responsibility for the content of the publication.





515 References

- Alin, A.: Multicollinearity, Wiley Interdisciplinary Reviews; Computational Statistics, 2, https://doi.org/10.1002/wics.84, 2010.
- Andreoli, R. V. and Kayano, M. T.: ENSO-related rainfall anomalies in South America and associated circulation features during warm and cold Pacific decadal oscillation regimes, International Journal of Climatology, 25, 2017–2030, https://doi.org/10.1002/JOC.1222;PAGE:STRING:ARTICLE/CHAPTER, 2005.
- Ayala, A., Pellicciotti, F., MacDonell, S., McPhee, J., Vivero, S., Campos, C., and Egli, P.: Modelling the hydrological response of debris-free and debris-covered glaciers to present climatic conditions in the semiarid Andes of central Chile, Hydrological Processes, 30, 4036–4058, https://doi.org/10.1002/hyp.10971, 2016.
 - Ayala, Á., Farías-Barahona, D., Huss, M., Pellicciotti, F., McPhee, J., and Farinotti, D.: Glacier runoff variations since 1955 in the Maipo River basin, in the semiarid Andes of central Chile, Cryosphere, 14, 2005–2027, https://doi.org/10.5194/tc-14-2005-2020, 2020.
- Barcaza, G., Nussbaumer, S. U., Tapia, G., Valdés, J., García, J. L., Videla, Y., Albornoz, A., and Arias, V.: Glacier inventory and recent glacier variations in the Andes of Chile, South America, Annals of Glaciology, 58, 166–180, https://doi.org/10.1017/aog.2017.28, 2017.
 - Boisier, J. P., Rondanelli, R., Garreaud, R. D., and Muñoz, F.: Anthropogenic and natural contributions to the Southeast Pacific precipitation decline and recent megadrought in central Chile, Geophysical Research Letters, 43, 413–421, 2016.
- Bond, T. C., Doherty, S. J., Fahey, D. W., Forster, P. M., Berntsen, T., Deangelo, B. J., Flanner, M. G., Ghan, S., Kärcher, B., Koch, D., Kinne, S., Kondo, Y., Quinn, P. K., Sarofim, M. C., Schultz, M. G., Schulz, M., Venkataraman, C., Zhang, H., Zhang, S., Bellouin, N., Guttikunda, S. K., Hopke, P. K., Jacobson, M. Z., Kaiser, J. W., Klimont, Z., Lohmann, U., Schwarz, J. P., Shindell, D., Storelvmo, T., Warren, S. G., and Zender, C. S.: Bounding the role of black carbon in the climate system: A scientific assessment, Journal of Geophysical Research Atmospheres, 118, https://doi.org/10.1002/jgrd.50171, 2013.
 - Breusch, T. S. and Godfrey, L. G.: Data Transformation Tests, The Economic Journal, 96, https://doi.org/10.2307/2232969, 1986.
- Breusch, T. S. and Pagan, A. R.: The Lagrange Multiplier Test and its Applications to Model Specification in Econometrics, The Review of Economic Studies, 47, https://doi.org/10.2307/2297111, 1980.
 - Burman, P.: A comparative study of ordinary cross-validation, v-fold cross-validation and the repeated learning-testing methods, Biometrika, 76, https://doi.org/10.1093/biomet/76.3.503, 1989.
- Caro, A., Gimeno, F., Rabatel, A., Condom, T., and Ruiz, J. C.: Glacier clusters identification across Chilean Andes using topo-climatic variables, Investigaciones Geográficas, p. 119, 2020.
 - Casassa, G., López, P., Pouyaud, B., and Escobar, F.: Detection of changes in glacial run-off in alpine basins: examples from North America, the Alps, central Asia and the Andes, Hydrological Processes: An International Journal, 23, 31–41, 2009.
 - Cereceda-Balic, F., Vidal, V., Moosmüller, H., and Lapuerta, M.: Reduction of snow albedo from vehicle emissions at Portillo, Chile, Cold Regions Science and Technology, 146, 43–52, https://doi.org/10.1016/j.coldregions.2017.11.008, 2018.
- Cereceda-Balic, F., Gorena, T., Soto, C., Vidal, V., Lapuerta, M., and Moosmüller, H.: Optical determination of black carbon mass concentrations in snow samples: A new analytical method, Science of the Total Environment, https://doi.org/10.1016/j.scitotenv.2019.133934, 2019.
 - Cereceda-Balic, F., Vidal, V., Ruggeri, M. F., and González, H. E.: Black carbon pollution in snow and its impact on albedo near the Chilean stations on the Antarctic peninsula: First results, Science of the Total Environment, 743, https://doi.org/10.1016/j.scitotenv.2020.140801, 2020.



565



- Cereceda-Balic, F., Ruggeri, M. F., Vidal, V., Ruiz, L., and Fu, J. S.: Understanding the role of anthropogenic emissions in glaciers retreat in the central Andes of Chile, Environmental Research, 214, https://doi.org/10.1016/j.envres.2022.113756, 2022.
- CETAM: Centro de Tecnologías Ambientales UTFSM: Caracterización glacioquímica de elementos traza en muestras de nieve, Tech. rep., Ministerio de Obras Públicas, Valparaíso, 2014.
- Chen, J., Zhu, X., Vogelmann, J. E., Gao, F., and Jin, S.: A simple and effective method for filling gaps in Landsat ETM+ SLC-off images, Remote Sensing of Environment, 115, https://doi.org/10.1016/j.rse.2010.12.010, 2011.
 - Chinn, T., Winkler, S., Salinger, M. J., and Haakensen, N.: Srecent glacier advances in Norway and New Zealand: A comparison of their glaciological and meteorological causes, Geografiska Annaler, Series A: Physical Geography, 87, https://doi.org/10.1111/j.0435-3676.2005.00249.x, 2005.
- 560 Cook, D. and Weisberg, S.: An Introduction to Regression Graphics, John Wiley & Sons, 1994.
 - Cordero, R. R., Rowe, P. M., Damiani, A., MacDonell, S., Carrasco, J., Feron, S., et al.: Black carbon in the Southern Andean snowpack, Environmental Research Letters, 17, 044 026, https://doi.org/10.1088/1748-9326/ac5df0, 2022.
 - Dangles, O., Rabatel, A., Kraemer, M., Zeballos, G., Soruco, A., and D., J.: Ecosystem sentinels for climate change? Evidence of wetland cover changes over the last 30 years in the tropical Andes, PLoS ONE, 12(5), https://doi.org/https://doi.org/10.1371/journal.pone.0175814, 2017.
 - DGA: Diagnóstico y clasificación de los Cursos y cuerpos de agua Según objetivos de calidad. Cuenca del Rio Maipo, Ministerio Obras Públicas de Chile, pp. 1–105, https://mma.gob.cl/wp-content/uploads/2017/12/Maipo.pdf, 2004.
 - DGA: Variaciones Recientes de Glaciares en Chile, según principales zonas glaciológicas, Tech. rep., Ministerio de Obras Públicas, 2011. DGA: Inventario Nacional de Glaciares 2014, Tech. rep., Ministerio de Obras Públicas, 2014.
- 570 DGA: Inventario Público de Glaciares, actualización 2022, 2022.
 - Dozier, J.: Spectral signature of alpine snow cover from the landsat thematic mapper, Remote Sensing of Environment, 28, 9–22, https://doi.org/10.1016/0034-4257(89)90101-6, 1989.
 - Durbin, J. and Watson, G. S.: Testing for serial correlation in least squares regression. II., Biometrika, 38, https://doi.org/10.1093/biomet/38.1-2.159, 1951.
- Dussaillant, I., Berthier, E., Brun, F., Masiokas, M., Hugonnet, R., Favier, V., Rabatel, A., Pitte, P., and Ruiz, L.: Two decades of glacier mass loss along the Andes, Nature Geoscience, 12, https://doi.org/10.1038/s41561-019-0432-5, 2019.
 - Escanilla-Minchel, R., Alcayaga, H., Soto-Alvarez, M., Kinnard, C., and Urrutia, R.: Evaluation of the Impact of Climate Change on Runoff Generation in an Andean Glacier Watershed, Water, 12, https://doi.org/10.3390/w12123547, 2020.
- Escobar, F. and Aceituno, P.: Influencia del fenómeno ENSO sobre la precipitación nival en el sector andino de Chile Central durante el invierno, Bulletin de l'Institute Français d'Études Andines, 27, 753–759, 1998.
 - Evans, D. J.: 8.27 Geomorphology and Retreating Glaciers, in: Treatise on Geomorphology, edited by Shroder, J. F., pp. 460–478, Academic Press, San Diego, https://doi.org/10.1016/B978-0-12-374739-6.00225-6, 2013.
 - Farías-Barahona, D., Vivero, S., Casassa, G., Schaefer, M., Burger, F., Seehaus, T., Iribarren-Anacona, P., Escobar, F., and Braun, M. H.: Geodetic mass balances and area changes of Echaurren Norte Glacier (Central Andes, Chile) between 1955 and 2015, Remote Sensing, 11, https://doi.org/10.3390/rs11030260, 2019.
 - Farías-Barahona, D., Wilson, R., Bravo, C., Vivero, S., Caro, A., Shaw, T. E., Casassa, G., Ayala, Á., Mejías, A., Harrison, S., Glasser, N. F., McPhee, J., Wündrich, O., and Braun, M. H.: A near 90-year record of the evolution of El Morado Glacier and its proglacial lake, Central Chilean Andes, Journal of Glaciology, pp. 1–15, https://doi.org/10.1017/jog.2020.52, 2020.



600

605

615



- Flemming, J., Benedetti, A., Inness, A., Engelen J, R., Jones, L., Huijnen, V., Remy, S., Parrington, M., Suttie, M., Bozzo, A., Peuch, V. H.,
 Akritidis, D., and Katragkou, E.: The CAMS interim Reanalysis of Carbon Monoxide, Ozone and Aerosol for 2003-2015, Atmospheric
 Chemistry and Physics, 17, https://doi.org/10.5194/acp-17-1945-2017, 2017.
 - Garreaud, R. D., Vuille, M., Compagnucci, R., and Marengo, J.: Present-day South American climate, Palaeogeography, Palaeoclimatology, Palaeoecology, 281, 180–195, https://doi.org/10.1016/J.PALAEO.2007.10.032, 2009.
- Garreaud, R. D., Alvarez-Garreton, C., Barichivich, J., Pablo Boisier, J., Christie, D., Galleguillos, M., LeQuesne, C., McPhee, J., and Zambrano-Bigiarini, M.: The 2010-2015 megadrought in central Chile: Impacts on regional hydroclimate and vegetation, Hydrology and Earth System Sciences, 21, https://doi.org/10.5194/hess-21-6307-2017, 2017.
 - Garreaud, R. D., Boisier, J. P., Rondanelli, R., Montecinos, A., Sepúlveda, H. H., and Veloso-Aguila, D.: The Central Chile Mega Drought (2010–2018): A climate dynamics perspective, International Journal of Climatology, 40, 421–439, https://doi.org/10.1002/joc.6219, 2020.
 - Ghosh, J. K., Delampady, M., and Samanta, T.: An introduction to Bayesian analysis: theory and methods, vol. 725, New York: Springer, 2006.
 - Gramsch, E., Muñoz, A., Langner, J., Morales, L., Soto, C., Pérez, P., and Rubio, M. A.: Black carbon transport between Santiago de Chile and glaciers in the Andes Mountains, Atmospheric Environment, 232, https://doi.org/10.1016/j.atmosenv.2020.117546, 2020.
 - Granier, C., Darras, S., Denier van der Gon, H., Doubalova, J., Elguindi, N., Galle, B., Gauss, M., Guevara, M., Jalkanen, J.-P., Kuenen J., Liousse, C., Quack, B., Simpson, D., and Sindelarova, K.: The Copernicus Atmosphere Monitoring Service global and regional emissions (April 2019 version), Tech. rep., ECMWF, https://doi.org/http://doi.org/10.24380/d0bn-kx16, 2019.
 - Hernandez, D., Mendoza, P. A., Boisier, J. P., and Ricchetti, F.: Hydrologic Sensitivities and ENSO Variability Across Hydrological Regimes in Central Chile (28°–41°S), Water Resources Research, 58, e2021WR031860, https://doi.org/10.1029/2021WR031860, 2022.
 - Hoaglin, D. C. and Welsch, R. E.: The hat matrix in regression and anova, American Statistician, 32, https://doi.org/10.1080/00031305.1978.10479237, 1978.
- Kang, S., Zhang, Y., Qian, Y., and Wang, H.: A review of black carbon in snow and ice and its impact on the cryosphere, Earth-Science Reviews, p. 103346, https://doi.org/10.1016/j.earscirev.2020.103346, 2020.
 - Kendall, M. G.: Rank Correlation Methods., Biometrika, 44, https://doi.org/10.2307/2333282, 1957.
 - Le Quesne, C., Acuña, C., Boninsegna, J. A., Rivera, A., and Barichivich, J.: Long-term glacier variations in the Central Andes of Argentina and Chile, inferred from historical records and tree-ring reconstructed precipitation, Palaeogeography, Palaeoclimatology, Palaeoecology, 281, https://doi.org/10.1016/j.palaeo.2008.01.039, 2009.
 - Li, X., Kang, S., Sprenger, M., Zhang, Y., He, X., Zhang, G., Tripathee, L., Li, C., and Cao, J.: Black carbon and mineral dust on two glaciers on the central Tibetan Plateau: Sources and implications, Journal of Glaciology, 66, 248–258, https://doi.org/10.1017/jog.2019.100, 2020.
 - Lo Vecchio, A., Candela, M., Falaschi, D., Otero, F., Videla, M. A., Lenzano, M. G., and Rivera, A.: Cambio de área glaciar en el volcán Maipo (Andes Centrales), una aproximación morfométrica: 4 décadas de registros satelitales, Andean Geology, 49, 55–76, https://doi.org/10.5027/andgeov49n1-3369, 2022.
 - Malmros, J. K., Mernild, S. H., Wilson, R., Yde, J. C., and Fensholt, R.: Glacier area changes in the central Chilean and Argentinean Andes 1955-2013/14, Journal of Glaciology, https://doi.org/10.1017/jog.2016.43, 2016.
 - Mann, H. B.: Nonparametric Tests Against Trend, Econometrica, 13, https://doi.org/10.2307/1907187, 1945.
- Marangunic, C.: Inventario de glaciares: Hoya del Río Maipo, Tech. rep., Ministerio de Obras Públicas, Dirección General de Aguas (DGA), 625 1979.



635

645



- Masiokas, M. H., Villalba, R., Luckman, B. H., Le Quesne, C., and Aravena, J. C.: Snowpack variations in the central Andes of Argentina and Chile, 1951-2005: Large-scale atmospheric influences and implications for water resources in the region, Journal of Climate, 19, 6334–6352, https://doi.org/10.1175/JCLI3969.1, 2006.
- Masiokas, M. H., Rabatel, A., Rivera, A., Ruiz, L., Pitte, P., Ceballos, J. L., Barcaza, G., Soruco, A., Bown, F., Berthier, E., Dussail-lant, I., and MacDonell, S.: A Review of the Current State and Recent Changes of the Andean Cryosphere, Frontiers in Earth Science, https://doi.org/10.3389/feart.2020.00099, 2020.
 - McCarthy, M., Meier, F., Fatichi, S., Stocker, B. D., Shaw, T. E., Miles, E., et al.: Glacier contributions to river discharge during the current Chilean megadrought, Earth's Future, 10, e2022EF002852, https://doi.org/10.1029/2022EF002852, 2022.
 - Mendez, J., Ramirez, A., Zarate, A., and Cavazos, T.: Teleconexiones de la Oscilación Decadal del Pacífico (PDO) a la precipitación y temperatura en México, Investigaciones geográficas, 73, https://doi.org/https://doi.org/10.14350/rig.23862, 2011.
 - Mernild, S. H., Beckerman, A. P., Yde, J. C., Hanna, E., Malmros, J. K., Wilson, R., and Zemp, M.: Mass loss and imbalance of glaciers along the Andes Cordillera to the sub-Antarctic islands, Global and Planetary Change, 133, 109–119, https://doi.org/10.1016/j.gloplacha.2015.08.009, 2015.
- Migliavacca, F., Confortola, G., Soncini, A., Senese, A., Diolaiuti, G. A., Smiraglia, C., Barcaza, G., Bocchiola, D., et al.: Hydrology and potential climate changes in the Rio Maipo (Chile), Geografia Fisica e Dinamica Quaternaria, 38, 155–168, 2015.
 - Ming, J., Xiao, C., Cachier, H., Qin, D., Qin, X., Li, Z., and Pu, J.: Black Carbon (BC) in the snow of glaciers in west China and its potential effects on albedos, Atmospheric Research, 92, 114–123, https://doi.org/10.1016/j.atmosres.2008.09.007, 2009.
 - Núñez, J., Rivera, D., Oyarzún, R., and Arumí, J. L.: Influence of Pacific Ocean multidecadal variability on the distributional properties of hydrological variables in north-central Chile, Journal of Hydrology, 501, 227–240, https://doi.org/10.1016/J.JHYDROL.2013.07.035, 2013.
 - Ohlanders, N., Rodriguez, M., and McPhee, J.: Stable water isotope variation in a Central Andean watershed dominated by glacier and snowmelt, Hydrology and Earth System Sciences, 17, 1035–1050, 2013.
 - Pettitt, A. N.: A Non-Parametric Approach to the Change-Point Problem, Applied Statistics, 28, https://doi.org/10.2307/2346729, 1979.
- Prabhu, V., Soni, A., Madhwal, S., Gupta, A., Sundriyal, S., Shridhar, V., Sreekanth, V., and Mahapatra, P. S.: Black carbon and biomass burning associated high pollution episodes observed at Doon valley in the foothills of the Himalayas, Atmospheric Research, 243, 105 001, https://doi.org/10.1016/j.atmosres.2020.105001, 2020.
 - Qu, B., Ming, J., Kang, S. C., Zhang, G. S., Li, Y. W., Li, C. D., Zhao, S. Y., Ji, Z. M., and Cao, J. J.: The decreasing albedo of the Zhadang glacier on western Nyainqentanglha and the role of light-absorbing impurities, Atmospheric Chemistry and Physics, 14, 11117–11128, https://doi.org/10.5194/acp-14-11117-2014, 2014.
- Rabatel, A., Castebrunet, H., Favier, V., Nicholson, L., and Kinnard, C.: Glacier changes in the Pascua-Lama region, Chilean Andes (29 S): recent mass balance and 50 yr surface area variations, The Cryosphere, 5, 1029–1041, 2011.
 - Raina, V.: Himalayan Glaciers: A State-of-Art Review of Glacial Studies, Glacial Retreat and Climate Change, Tech. rep., Geological Survey of India, 2009.
 - Rivera, A., Acuña, C., and Casassa, G.: Glacier Variations in Central Chile (32°S-41°S), in: Glacier Science and Environmental Change, chap. Forty-Nine, pp. 246–247, John Wiley and Sons, Ltd, https://doi.org/10.1002/9780470750636.ch49, 2006.
 - Rodriguez, M., Ohlanders, N., Pellicciotti, F., Williams, M. W., and McPhee, J.: Estimating runoff from a glacierized catchment using natural tracers in the semi-arid Andes cordillera, Hydrological processes, 30, 3609–3626, 2016.
 - Segovia Rocha, A. and Videla Giering, Y.: Caracterización glaciológica de Chile Glaciological, Investigaciones geográficas, 53, 3-24, 2017.





- Seheult, A. H., Green, P. J., Rousseeuw, P. J., and Leroy, A. M.: Robust Regression and Outlier Detection., Journal of the Royal Statistical Society. Series A (Statistics in Society), 152, https://doi.org/10.2307/2982847, 1989.
 - Shapiro, S. S. and Wilk, M. B.: An Analysis of Variance Test for Normality (Complete Samples), Biometrika, 52, https://doi.org/10.2307/2333709, 1965.
 - Shaw, T. E., Ulloa, G., Farías-Barahona, D., Fernandez, R., Lattus, J. M., and McPhee, J.: Glacier albedo reduction and drought effects in the extratropical Andes, 1986–2020, Journal of Glaciology, 67, 158–169, https://doi.org/10.1017/jog.2020.99, 2021.
- 670 Shi, Y. and Liu, X.: Dust Radiative Effects on Climate by Glaciating Mixed-Phase Clouds, Geophysical Research Letters, 46, https://doi.org/10.1029/2019GL082504, 2019.
 - Trenberth, K. E.: The Definition of El Niño, Bulletin of the American Meteorological Society, 78, 2771–2778, https://doi.org/10.1175/1520-0477(1997)078<2771:TDOENO>2.0.CO;2, 1997.
- Valdés-Pineda, R., Pizarro, R., García-Chevesich, P., Valdés, J. B., Olivares, C., Vera, M., Balocchi, F., Pérez, F., Vallejos, C., Fuentes, R., et al.: Water governance in Chile: Availability, management and climate change, Journal of Hydrology, 519, 2538–2567, 2014.
 - Vicencio, J., Zuleta, M., and Vásquez, R.: Eventos de nieve en Santiago de Chile / Snow events in Santiago de Chile, Tech. rep., Dirección Metereológica de Chile, 2017.
 - Vincent, C.: Influence of climate change over the 20th Century on four French glacier mass balances, Journal of Geophysical Research Atmospheres, 107, https://doi.org/10.1029/2001JD000832, 2002.
- Wang, Z., Huang, X., and Ding, A.: Dome effect of black carbon and its key influencing factors: A one-dimensional modelling study, Atmospheric Chemistry and Physics, 18, https://doi.org/10.5194/acp-18-2821-2018, 2018.
 - Wiltshire, A. J.: Climate change implications for the glaciers of the Hindu Kush, Karakoram and Himalayan region, Cryosphere, 8, https://doi.org/10.5194/tc-8-941-2014, 2014.
- Zhang, Y., Gao, T., Kang, S., Sprenger, M., Tao, S., Du, W., Yang, J., Wang, F., and Meng, W.: Effects of black carbon and mineral dust on glacial melting on the Muz Taw glacier, Central Asia, Science of the Total Environment, 740, https://doi.org/10.1016/j.scitotenv.2020.140056, 2020.